RSC Advances

REVIEW

View Article Online
View Journal | View Issue

Cite this: *RSC Adv.*, 2026, **16**, 7777

Multifaceted boron nitride nanomaterials: a comprehensive review of synthesis, property engineering and multidisciplinary applications

Reveka Kushwah,†[a] Samy G. Alamir, †[ab] Sulaiman Al-Sulaimi,[c] Ahmed Al-Harrasi [a] and Adel Ehab Ibrahim *[ad]

Boron nitride (BN) nanomaterials, spanning zero-dimensional (0D) quantum dots, 1D nanotubes, 2D nanosheets, 3D and macroscopic architectures, have garnered emerging attention as functional analogs to carbon-based nanomaterials. Their wide band gap, high thermal conductivity, electrical insulation, and chemical inertness make them versatile candidates for advanced technologies. This review highlights the synthesis–structure–function relationships achieved through top–down methods, such as exfoliation and ball milling, and bottom–up strategies, including chemical vapor deposition and plasma processing. Defect engineering, dopant incorporation, and surface functionalization are further discussed as key levers for tailoring BN nanomaterials' optical, electronic, and interfacial behavior. The review also explores the diverse range of BN nanomaterial applications across various disciplines, such as chemical analysis, biomedicine, catalysis, energy, and aerospace. The recent advances highlight opportunities for data-driven strategies coupled with *operando* characterization to control and optimize composition, morphology, and defect chemistry. These developments are expected to accelerate translation into practical technologies across wide applications.

Received 8th December 2025
Accepted 28th January 2026

DOI: 10.1039/d5ra09482h

rsc.li/rsc-advances

1 Introduction

Nanomaterials, typically defined as having at least one dimension in the 1–100 nm range, have garnered substantial attention due to their broad spectrum of applications. At the nanoscale, size-, shape-, and surface-dependent phenomena emerge, including electron and phonon confinement, high specific surface areas, and abundant interfacial sites. These features enable unusual optical responses, rapid interfacial charge/energy transfer, and tunable chemisorption, resulting in properties that diverge markedly from their bulk counterparts. Nanoparticles exhibit diverse morphologies, each imparting some distinct physicochemical properties. Their performance is dictated by the synthesis–structure–function relationship, where fabrication route (top–down or bottom–up) determines defect motifs, crystallinity, and morphology. Moreover, defect/dopant engineering tunes electronic states and catalytic sites, while surface functionalization controls wettability, dispersibility, and recognition. In practice, synthesis strategies manipulate precursor type, pH, and temperature through a wide range of physical and chemical mechanisms, with additional considerations of scalability, reproducibility, and standardized metrology for optical, thermal, mechanical, and interfacial properties.[1] Although rigorous scientific investigation of nanomaterials is relatively recent, materials with nanoscale features have been unknowingly exploited for centuries. Across nanomaterial classes, carbon-based systems are widely applied in bioimaging, biosensing, electronic sensing,[2–7] composite reinforcement and cancer therapy,[8,9] light-emitting diodes,[10,11] photocatalysis,[12,13] analytical chemistry,[14,15] and aerospace technologies,[16,17] with new applications continually emerging.

Within the nanomaterials landscape, boron nitride (BN, White graphene) occupies a strategic niche, combining diverse advantages. Since their initial discovery in the 19th century, BN nanomaterials have experienced significant developments with marked advancements in their synthesis techniques and diverse applications. These materials have gained attraction in various fields, owing to their unique properties, such as thermal stability and electrical insulation. To provide a comprehensive overview of this progress, SI Table S1 was compiled to highlight some key periods and landmarks in their advancements in synthesis and application, illustrating their important transformation for both research and industry.

[a]*Natural and Medical Sciences Research Center, University of Nizwa, Birkat Al Mauz 616, Nizwa city, Oman. E-mail: reveka.kushwah@unizwa.edu.om; aharrasi@unizwa.edu.om*

[b]*Pharmaceutical Analytical Chemistry Department, Faculty of Pharmacy, Ain Shams University, Abassia 11566, Cairo, Egypt. E-mail: sami.goerge@pharma.asu.edu.eg*

[c]*Department of Biological Science and Chemistry, University of Nizwa, Birkat Al Mauz 616, Nizwa, Oman. E-mail: s.salimi@unizwa.edu.om*

[d]*Pharmaceutical Analytical chemistry Department, Faculty of Pharmacy, Port-Said University, Port-Said 42511, Egypt. E-mail: adel.ehab@pharm.psu.edu.eg*

† These authors contributed equally to this work.

BN is an inorganic compound of boron (B, group 13) and nitrogen (N, group 15) atoms that belongs to the III–V family, has a wide band gap (5–6 eV), and can adopt sp^2 or sp^3 bonding frameworks with ionic character.[18–21] In 1842, Balmain first synthesized BN through the reaction of molten H_3BO_3 with potassium cyanide.[22] BN combines high oxidation resistance and thermal stability (up to ~900 °C) with high thermal conductivity,[23–26] intrinsic electrical insulation,[27] exceptional rigidity,[28] hydrophobicity, high specific surface area, photoluminescence, chemical inertness,[29–31] and comparatively low cytotoxicity compared with other nanomaterials and boron-containing compounds.[32]

Often termed "white graphene", BN possesses an ordered structure comparable to graphene and has a crystal structure similar to that of carbon. Unlike graphene's purely covalent bonds, the B–N bonds possess an ionic character. The electronegativity difference between B and N drives charge transfer from B to N, imparting strong bond polarity and rendering BN an electrical insulator whose characteristics remain tunable *via* doping, alloying, functionalization, and heterostructuring.[33,34] BN appears in four crystalline allotropes, where electrostatic interlayer interactions dictate stacking: hexagonal (h-BN, graphite-like, AB stacking, $P6_3/mmc$), rhombohedral (r-BN, graphite-like, ABC stacking, $R\text{-}3m$), cubic (c-BN, zinc blende structure, $F\text{-}43m$), and wurtzite (w-BN, lonsdaleite-like, $P6_3mc$). In h-BN, AB stacking places B atoms in one layer above N atoms in the adjacent layer, consistent with $P6_3/mmc$ symmetry.[35,36] The stacked layers are held together by van der Waals interactions, with an interlayer spacing of ~0.333 nm.[7,37] While h-BN is typically synthesized at elevated temperatures near ambient pressure, theoretical and experimental studies indicate that c-BN is kinetically more stable than h-BN under high-pressure, ambient-temperature conditions.[28] h-BN exhibits excellent biocompatibility and electronic properties, as detailed by Cao *et al.*, and its atomically precise AB stacking in few-layer and heterostructure configurations renders it highly attractive for electronic device applications.[38,39] Fig. 1 summarizes the BN phase diagram and structural models of its allotropes across different dimensionalities.

BN nanomaterials are accessible *via* top–down exfoliation/milling and bottom–up growth (*e.g.*, chemical vapor deposition (CVD), solvothermal, polymer-derived ceramic routes).[40] Recent advances in synthesis and a deeper understanding of BN properties have enabled diverse nanostructured forms, including nanoparticles, nanoribbons, nanofibers, nanosheets, nanotubes, and nanocomposites, with composite classes delineated by matrix (polymer-*vs.* ceramic-based) routinely characterized by transmission electron microscopy, scanning electron microscopy, energy-dispersive X-ray spectroscopy, and X-ray diffraction. Across dimensionalities, BN occurs as zero-dimensional (0D) (BN quantum dots (BNQDs), nanospheres), 1D (nanotubes (BNNTs), nanoribbons, nanofibers), 2D nanosheets/films (BNNSs), and 3D (porous monoliths/aerogels/lattices/composites).

Beyond architectural dimensionality, surface chemistry and intrinsic defects provide key design levers for BN nanomaterials. Because their properties are highly surface-dependent, effective tailoring requires careful selection of functionalization strategies. Defects/dopants (B/N vacancies; edge –OH/–NH_x; –R/–OR/–C/–O/–S/–F incorporation) and surface chemistry govern band-edge/defect emissions in BNQDs, adsorption energetics in porous BN, and interfacial compatibility in composites and biointerfaces.[34,41–43] Functionalization can be achieved efficiently through methods such as thermal oxidation in air or sonication,[41,42] with hydroxyl groups frequently being covalently attached to B sites. Hydroxylated BN nanosheets and nanotubes, prepared *via* both top–down and bottom–up approaches, have been reported by Ren and Stagi.[44]

Translating these properties and their tunable surface and defect chemistries into practice, recent work explores BN nanostructures and BN-semiconductor hybrids (utilizing BN as a dielectric/support/encapsulation material), aiming to address global challenges in energy and environmental remediation. BN nanomaterials also show promise in drug delivery, especially in controlled-release systems,[45,46] as well as in optoelectronics,[47] thermal management,[48] and two-dimensional device architectures.[34]

Functionally, BN's chemical/oxidative stability, wide band gap, very low optical background, and intrinsic electrical insulation make it a pinhole-free dielectric spacer in spectroscopic/electronic architectures (enabling controlled non-radiative energy transfer (NRET)/metal-enhanced fluorescence (MEF)). It also serves as a robust catalyst/catalyst-support (*e.g.*, oxidative dehydrogenation, CO_2 conversion), a selective adsorbent for remediation and gas purification even under extreme conditions, a modifier of stationary phases that enhances chromatographic resolution/detection, and a thermally conductive yet insulating filler for composites; these properties also address challenges in electrochemical systems (electrocatalyst contamination, anode contact, separator stability) and support water treatment through porous BN, which can remove dyes, organic solvents, and heavy metal ions.[49]

Several reviews survey BN synthesis and applications,[34,50–57] including one- and two-dimensional BN,[35] nanoscale BN from molecular precursors,[58] and BN for environmental remediation.[36] This review offers a unique multi-dimensional perspective on boron nitride nanomaterials where it systematically organize recent advances in synthesis strategies to BN dimensionalities (0D through 3D and macroscopic architectures), link fabrication methods to each BN form's properties and functions, emphasize design rules such as defects/dopants engineering and surface functionalization to performance followed by recent developments across diverse fields (analytical chemistry, biomedicine, catalysis, energy, materials science). Unlike previous reviews which may focus on a single aspect (synthesis or a specific application area), the review integrates synthesis strategies, property engineering and a broad spectrum of applications in one continuum to emphasize on emerging and underrepresented areas (*e.g.*, BN in analytical sensing and in energy storage), offer a unified perspective intended to guide researchers in bridging fundamental BN nano-chemistry with practical implementations, and provide a clear up-to-date roadmap for future BN research and development.

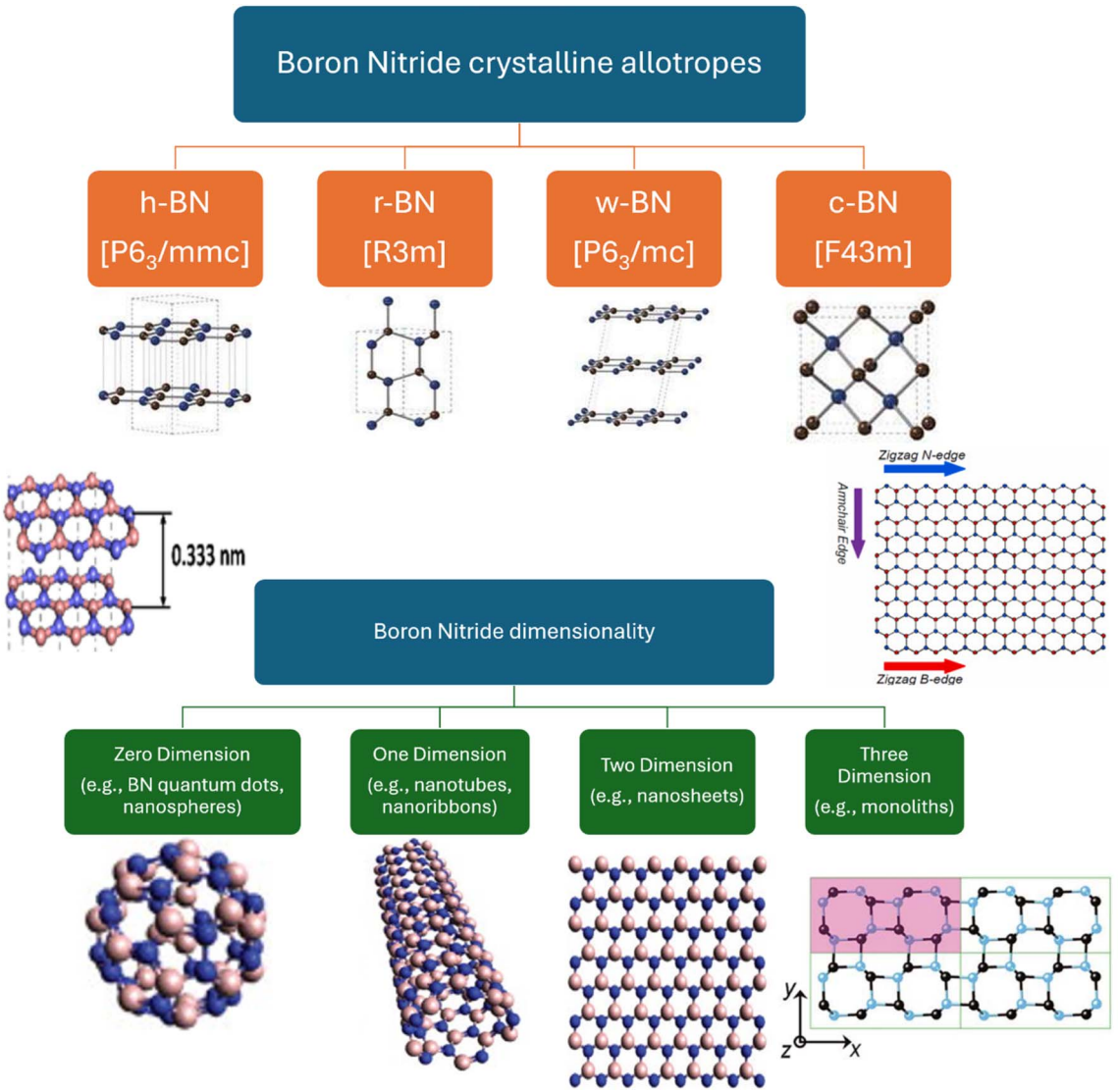

Fig. 1 Different BN allotropes and dimensionalities (0D–3D), laying out the taxonomy of BN nanomaterials.

2 Synthesis of boron nitride nanomaterials

Given their unique characteristics, BN-based materials have attracted considerable scientific interest. The characteristics of nanostructured BN-based materials vary, as do the synthesis methods. Each technique offers application-specific advantages, alongside inherent limitations. Recent BN preparation techniques, along with their benefits and drawbacks, were summarized by Pu and co-workers.[59]

Two standard methodologies are used to produce nanomaterials: top–down and bottom–up.[60] Top–down approaches reduce bulk materials to the nanoscale, whereas bottom–up approaches assemble atoms or molecules. The potential applications of nanomaterials depend on their physical, chemical, structural, and dimensional properties, which are, in turn, governed by the choice of precursor and the synthesis route.

Top–down methods rely on splitting/removal of bulk material or size reduction in large-scale processes to obtain the target structures and attributes. Most top-down techniques are physical (*e.g.*, ball milling, photolithography, X-ray lithography) and straightforward, but they offer limited control over particle size distribution, composition, and dimensions. Conversely, bottom–up approaches build materials block-by-block or layer-by-layer from atoms or molecules, enabling tailored compositions and morphologies for application-specific designs (*e.g.*, drug delivery). Physical processes can be energy-intensive and, in some cases, involve ionizing radiation, whereas chemical routes may employ hazardous precursors and generate toxic by-products, posing environmental and health risks.[61]

BN nanoparticles and BN-based composites are synthesized *via* liquid exfoliation, template-based or template-free routes, ball milling, sputtering, solvothermal/hydrothermal processes, wet-chemical synthesis, CVD, and polymer-derived ceramic pyrolysis. Representative physical and chemical methods are highlighted in Fig. 2. Focusing on recent developments, this review outlines fabrication methods for key BN architectures,

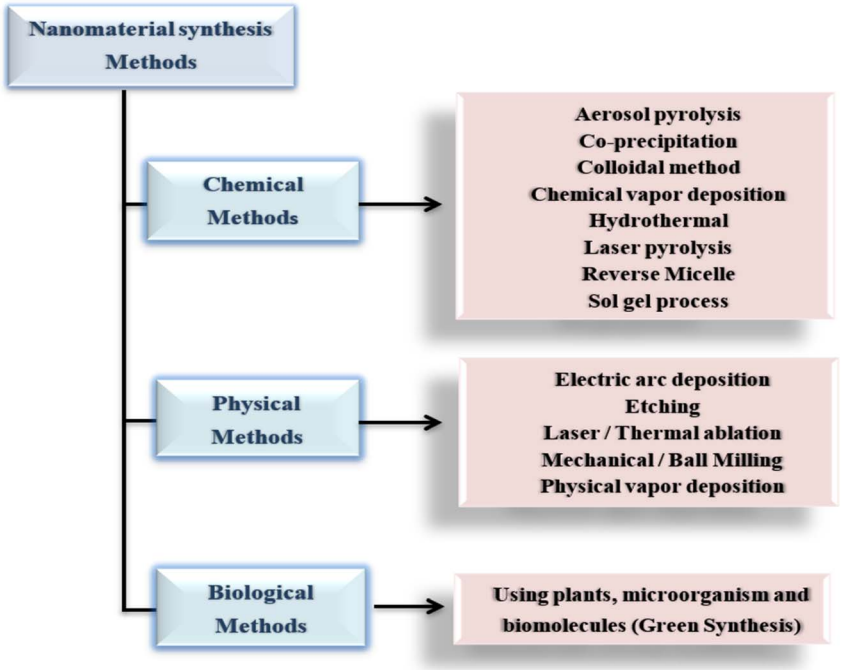

Fig. 2 Flowchart illustrating different synthesis techniques for BN nanomaterials.

including quantum dots (BNQDs), nanotubes (BNNTs), nanosheets (BNNSs), and macroscopic BN architectures.

2.1 Zero-dimensional BN: quantum dots

Further shrinking of 2D materials to the nanoscale yields zero-dimensional quantum dots (QDs). QDs, which are smaller than 10 nm, have attracted significant attention owing to their strong fluorescence, biocompatibility, chemical stability and photostability in both hydrophilic and hydrophobic media, facile doping and modification, high surface-to-volume ratios, and adaptability to diverse physicochemical environments,[62] conferring them advantages for bio-applications,[63] including diagnostics, biosensing, fluorescence imaging, metal ion detection, chemiluminescence (CL), electrochemiluminescence (ECL), and thermal sensing.[64] Advances in optical and electrochemical sensors using graphene QDs[65] have spurred interest and paved the way for the creation of graphene-like alternatives, including BNQDs and QDs of transition metals and their oxides.[66,67]

The controlled synthesis of BNQDs is essential for both fundamental studies of their quantum phenomena and their applications in various fields, including optics, electronics, biomedicine, and catalysis. BNQDs, which often emit blue light under UV irradiation, are reported to exhibit good biocompatibility, superior dispersibility, and low toxicity. BNQD preparation strategies are broadly classified into top–down and bottom–up approaches. Hydrothermal/solvothermal and exfoliation-based methods, employing various precursors and solvents under different temperatures and pressures, are widely adopted for BNQD synthesis, as shown in Fig. 3. Precursor selection and method choice depend on target quantum yield (QY), processing time, and scalability, among other factors.

BNQDs are usually fabricated using solvent-assisted or liquid-phase techniques. In top–down liquid exfoliation, bulk h-BN flakes are exfoliated and subsequently fragmented into BNQDs, followed by separation.[68–72] Liquid exfoliation offers a simple, safe, and environmentally friendly route to BNQDs. Typical solvents, including ethanol, *N*-methyl-2-pyrrolidone, and dimethylformamide, are chosen for their surface-energy compatibility. BNQDs synthesized by a combined liquid-exfoliation/solvothermal process exhibited good hydrophilicity and were readily integrated into polymer structures, enabling proton-exchange capability and enhancing water retention of polymer-based membranes.[73] BNQDs have also been produced by combining liquid-phase exfoliation with high-energy ultrasonication. Intense sonication produced few-layer BN nanostructures (median ~12 atomic layers) alongside BNQDs.[74] Stengl *et al.* employed high-intensity ultrasonic exfoliation of BN nanosheets to produce built-in BNQDs.[75] Ultrasonication of h-BN to h-BN nanosheets (h-BNNSs), followed by solvothermal cutting in dimethylformamide (180 °C, 12 h), yielded blue-emissive BNQDs with time- and temperature-dependent photoluminescence.[76] Microwave irradiation (10 min, 150 °C, 500 W) yielded ~300 nm lateral monolayer h-BNNSs together with homogeneous BNQDs (~3.2 nm).[77] Across these techniques, the conditions governing synthesis and size distribution could be summarized as solvent selection and the nature and intensity of the applied energy, which dictate the extent of layer delamination, fragmentation, and defect formation. For instance, when using solvents whose surface energy matches that of h-BN, such as *N*-methyl-2-pyrrolidone and dimethylformamide, efficient exfoliation/layer delamination is promoted resulting in thinner starting flakes that can be subsequently fragmented by ultrasonication/heat/microwave where milder conditions

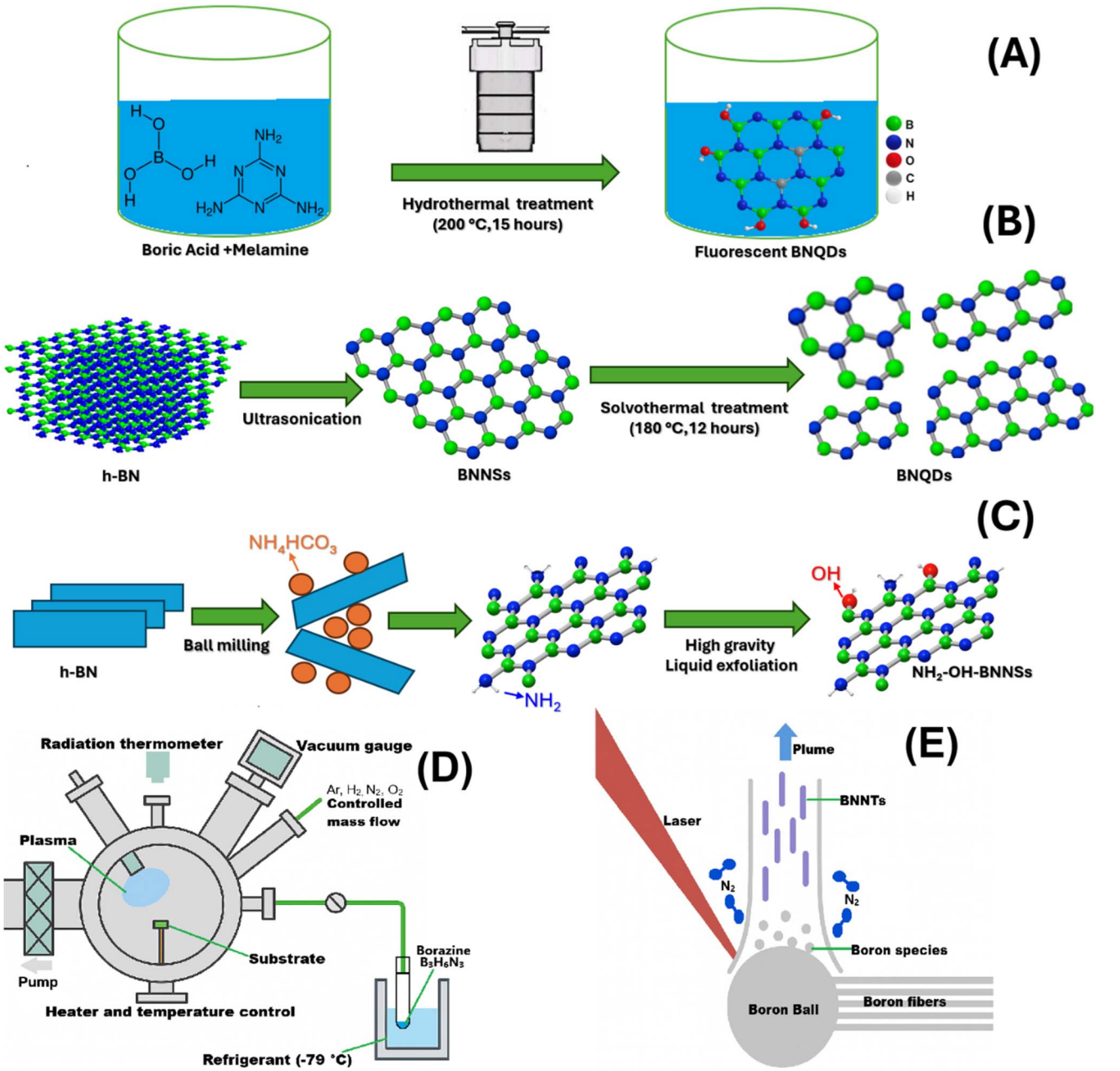

Fig. 3 Snippet figures illustrating different synthesis schematics for diverse BN morphologies; hydrothermal (A), solvothermal (B), liquid exfoliation (C), plasma-CVD (D), and laser ablation (E).

preserve larger lateral dimensions and the more powerful and longer duration of sonication/heating/irradiation will drive the BN toward smaller BNQDs and introduce defects that usually enhance photoluminescence and quantum yield, yet may also compromise crystalline integrity if over-generated. Notably, microwaves' rapid, uniform, and intense electromagnetic heating avoids prolonged thermal exposure that could induce extensive lattice damage. BNQDs synthesized by potassium intercalation exhibited a QY of 2.5%; the edge ratio of saturated sp^2 sites to dangling bonds critically influenced their properties at the nanoscale. These edge states are predicted to significantly influence the chemical and physical properties of h-BNNSs.[78] Owing to its van der Waals nature, basal-plane h-BN is intrinsically free of surface charge barriers and dangling bonds, whereas edges/defects can host dangling states.[79] By viewing the potassium intercalation pathway, the parameters affecting the synthesis and the generated BNQD characteristics could be interpreted. It is a sequence of chemical and thermal steps where at approximately 190–200 °C, potassium is inserted/intercalated into layered h-BN to weaken the interlayer van der Waals interactions and force the sheets apart then short air exposure triggers oxidative de-intercalation where potassium rapidly evaporates *in situ* to generate internal pressure and cleave the expanded layers into monolayer BN sheets and lastly any of ultrasonication/thermal/microwave treatment discussed earlier is used to complete their fragmentation into BNQDs.

Hence, raising the intercalation temperature or prolonging the soaking time intensifies layer separation which usually yields smaller-diameter quantum dots, albeit at the expense of creating a higher density of unsaturated edge sites which reflects the trade-offs between size reduction and defect generation.[80]

Moreover, an orthorhombic BNQD product was reported *via* solvothermal synthesis (ethanol; boric acid and cyanoguanidine as B/N sources), with XRD indicating an orthorhombic phase and high resolution transmission electron microscopy showing ~0.209 nm lattice spacing and 2–9 nm particle sizes;[81] This example shows the precursors role in bottom-up techniques where boric acid and cyanoguanidine breaking down produced B–N–C–O which acted as intermediates and dopants and influenced the lattice arrangements and defect configurations. In another study, blue-emitting h-BN QDs (3–7 nm) were synthesized from ammonia borane in carbon tetrachloride (180 °C); QLEDs fabricated from these QDs showed EL at 412 nm, red-shifted from their PL at 386 nm.[82] This also emphasize that solvents and precursors volatility are another factors that must be considered during synthesis because ammonia borane decomposing at low temperature (~100 °C) enables the controlled release of B–N species and influences nucleation and growth behavior, while the non-coordinating inert nature of carbon tetrachloride minimizes any side reactions or oxidation, thereby preserving the chemical purity of the nanostructures and reducing the tuning parameters to reaction temperature, duration and precursor concentration. Hydrothermal synthesis from boric acid and melamine produced ~4.6 nm BNQDs with oxygen-terminated edges that confer aqueous stability; subsequent solution-phase deposition yielded BNQD/ZnO heterointerfaces.[83] The study here further illustrates the influence of solution pH in surface chemistry where ammonia and amines are released upon melamine decomposition and buffers the solution toward mildly basic pH leading to surface amination and the formation –OH or $-O^-$ terminations at BNQDs edges rather than maintaining pure B–N bonds, which stabilized the blue fluorescence and improved aqueous dispersibility since the polar groups prevent restacking and enhance hydrogen-bonding with water, while at neutral pH fewer oxygenated edge sites would have been expected. This was also utilized to unlock broader BNQDs optoelectronic potential which was constrained by predominantly blue PL and generally low QYs. Strategies proposed to achieve full-color emission from modified BNQDs included solvothermal treatment following liquid exfoliation which yielded heat-resistant BNQDs (QY = 32.3%) and characterization suggested surface amination (NH_2 bound to BO_x^- species) that enhanced PL by improving surface states.[84] BNQDs and BNNS phosphors have also enabled multicolor LEDs with robust thermal stability.[85–87]

BNQD-based nanocomposites, with strong thermal and chemical resistance, are well-suited for electrode applications and separation membranes. Covalently bonded BNQD/reduced graphene oxide (rGO) hybrids improved charge-carrier concentration, electrolyte sorption, and durability, achieving a specific capacitance of 90 F g^{-1} at 1 A g^{-1}, thereby highlighting their promise as high-performance supercapacitor materials.[88] Hydrothermally synthesized BNQDs (boric acid/urea) exhibited blue fluorescence (~330 nm); Coating BNQDs onto a glassy-carbon electrode followed by electrochemical deposition of polyluminol produced a hybrid electrode with enhanced catalytic activity for vitamin C detection.[89] BNQDs incorporation into polyethersulfone membranes improved antifouling performance.[90] MTT and imaging assays consistently show low cytotoxicity and high biocompatibility for BNQDs; HeLa cells remain viable, internalize the dots *via* endocytosis, and exhibit no nuclear damage.[32] Collectively, these findings, combined with the inherent chemical and photostability of QDs, highlight BNQDs as promising candidates for diagnostics, biosensing, imaging, and separation membranes. As metal-free (Cd/Pb-free) QDs, they mitigate the heavy-metal toxicity associated with many II–VI systems and offer a more favorable biocompatibility profile.

2.2 One-dimensional BN: nanotubes and nanoribbons

Within the family of one-dimensional nanostructures, nanotubes are among the most extensively studied.[91] Considerable effort has been devoted to synthesizing superior boron nitride nanotubes (BNNTs). BN nanoribbons were produced by applying high pressure to BNNTs.[92] Chopra *et al.* first synthesized BNNTs in 1995 *via* plasma discharge between a BN-filled tungsten rod (in a carbon-free atmosphere) and a cooled copper electrode, a procedure similar to the carbon nanotube (CNT) plasma-arc methods.[93] Subsequent studies refined this production method.[94–96] Under pressurized N_2, high-temperature CO_2-laser ablation (Fig. 3) yields BNNTs through root growth from molten boron droplets or *via* open-end growth from BN radicals, the latter generally giving longer tubes.[97] In arc discharge and laser ablation syntheses, the applied energy and the N_2 gas pressure jointly dictate the dominant growth mode and, consequently, the morphology of the resulting BNNTs. At higher N_2 pressures, the growth typically proceeds through an open-end mechanism, in which reactive BN radicals are continuously incorporated at the nanotube tips, favoring longer nanotubes with smaller diameters formation whereas at lower N_2 pressure or when boron vapor preferentially condenses into molten droplets, a root-growth mechanism becomes more prominent. Under these conditions, nanotubes nucleate from boron droplets and extend outward, yielding multi-walled BNNTs that are shorter and wider. Beyond controlling morphology, sufficient energy input and optimized nitrogen pressure are also essential for suppressing amorphous by-products, turbostratic BN sheets, and particulate debris.

Chemical vapor deposition (CVD; Fig. 3), including boron-oxide-assisted CVD, has been employed to strike a balance between purity and yield in BNNT synthesis. However, BNNT synthesis can be hindered by high process temperatures (>1200 °C) and solid-state reactivity of boron precursors, among other reactive constraints. To address these challenges, multi-atmosphere thermal analysis with staged annealing was employed to monitor the solid-state reaction of the B/Li_2O system that concurrently acted as precursor, catalyst, and active component. Experimental data of this setup indicated that

lithium borate reduced reactant and ammonia consumption while maintaining high reactivity, efficiency, and flexibility.[98] In another study, multi-walled BNNTs have been synthesized by CVD using Fe_2O_3 catalyst and colemanite as the boron precursor where iron oxide is reduced *in situ* to metallic Fe or iron boride nanoparticles, which serve as active nucleation sites for BNNT growth, define the tube diameter (smaller catalyst particles seed thinner nanotubes), and enables synthesis at ~1050 °C which is comparatively lower than 1200 °C.[99] Both studies demonstrate that catalysts lower the required formation temperature and that optimizing the catalyst amount and temperature regulates BNNT wall thickness, structure, diameter uniformity, and purity, thereby aiding in the production of fewer amorphous boron impurities. Still, it has been noted that pinpointing the actual catalyst during BNNT growth is exceedingly difficult especially since high production rates of BNNTs and reduced amorphous-boron impurities suggest BN-radicals self-assembly.[100] Density Functional Theory-Molecular Dynamics simulations revealed that Li incorporation into the W_2B_5 lattice promotes the formation of a W–B–Li liquid and enhances compound vaporization, both of which are essential for effective BNNT growth; a three-component W–B–Li molecule can thus enable self-catalyzed, high-quality BNNT synthesis.[101] Aluminum-based catalysts have also been explored for CVD growth; AlB_2 has been identified as a key catalyst in BNNT synthesis.[102]

For plasma-based BNNT synthesis, the choice of feedstock, feed rate, and plasma power affects the crystalline quality of the product. Alrebh *et al.* used ammonia borane (melting and degradation temperatures ~62–127 °C) as an effective plasma feedstock, where the high AB flow/concentration increased BNNTs' yield and length, while the optimal plasma power ensured that BN radicals are efficiently incorporated into growing tubes rather than forming amorphous deposits. As a result, the enhanced boron-seed/BNNT-precursor formation yielded highly crystalline double-walled BNNTs with less turbostratic BN and negligible h-BN compared to h-BN powder feeds.[103] Plasma-assisted CVD from borazine over oxidized Cu nanoparticles yielded Cu-core/turbostratic-BN-shell nanotubes only when O_2 is present, with Cu_2O interlayer at the Cu/BN interface likely serving as the active catalyst.[104] In addition to the previously mentioned surface modifications, several reviews have surveyed BNNT production, covering advances in synthesis as well as doping and functionalization.[105]

Covalent or non-covalent modification of BNNTs enhances water dispersibility, stability, resistance to surface oxidation, and biological utility. Hence, functionalization with alkyl, alkoxy, or hydroxyl groups is a particularly promising strategy for improving BNNTs' aqueous solubility. Aguiar *et al.* functionalized B and N sites with carboxyl (–COOH) and hydroxyl (–OH) groups, altering the electron density and spin-polarized bands, inducing magnetic moments, reducing band gaps, and generating impurity-like flat bands. First-principles DFT of pristine single-walled BNNTs assessed high-coverage amino-acid functionalization (*e.g.*, glutamine, glycine, serine), showing increased partial charges, stable covalent bonding, more ionic B–N character, and polarity modulation, making them potential nanocarriers for drug delivery.[106,107] To improve BNNT dispersion, solvent-free covalent modification is necessary, as direct incorporation into polymers often leads to aggregation. Intercalation with amine groups combined with plant-based polyphenols (tannic acid, TA) produced BNNT-TA. Subsequent decylamine (DA) treatment yielded BNNT-TA-DA with enhanced interfacial reactivity toward polymers, addressing dispersion challenges. BNNT-TA and BNNT-TA-DA can be redispersed in both polar and nonpolar solvents, thereby improving their association and distribution in polymer matrices and overall composite performance. When 1 wt% BNNT-TA-DA was incorporated into epoxy, tensile strength increased by 26.8% and strain at break by 52.2% relative to neat epoxy.[108]

Unlike conductive CNTs, insulating BNNTs are suitable reinforcements in polymer matrices, heat dissipators, and protective coatings in harsh environments. BNNTs have applications in thermal management, optical/electronic devices, and as fillers in polymer composites. They have also been investigated for use in biocatalysis, biomedicine, water purification, and as protective shields and encapsulating materials.[50,109] Additionally, in aerospace, BNNTs are considered for spacesuits, shelters, and satellites, where materials must withstand extreme environmental conditions. The increasing miniaturization and multifunctionality of modern electronics lead to significant heat generation. Overheating can lead to severe electrical damage or even an explosion, making high-thermal-conductivity materials highly sought after. Composite materials with enhanced thermal conductivity have proven effective in thermal management and mitigating overheating. A BNNT/cellulose-nanofiber composite (25 wt% BNNTs) achieved $k = 21.39$ W m^{-1} K^{-1}.[110] A cellulose-nanocrystal composite with 20 wt% pristine BNNTs reached in-plane $k = 13.33$ W m^{-1} K^{-1}.[102] Composites formed by incorporating BNNTs with other materials confer exceptional strength while maintaining low weight. BNNT-reinforced aircraft wing plates exhibited enhanced mechanical properties, suggesting improved aerospace performance.[111]

Experiments showed that hexagonal BNNTs can act as atomically smooth nanocavities that sustain phonon-polariton whispering-gallery modes (enabled by low scattering losses and intrinsic hyperbolic dispersion), highlighting their promise for 1D photonic components.[112] BNNTs have also been incorporated into Li-ion battery electrolytes; at 0.9 wt% BNNT loading, Li-ion conductivity increased by ~30% and the transference number rose to ~0.73.[113] Bi_2Te_3-BNNT composite films support flexible thermoelectric, combining mechanical flexibility with thermal stability.[114]

2.3 Two-dimensional BN: nanosheets

Interest in boron nitride nanosheets (BNNSs) and related composites has surged in recent years owing to their multifunctionality, structural similarity to graphene, and potential applications in UV shielding, electrochemistry, and analytical chemistry.[115–117] Ares *et al.* experimentally validated theoretical predictions by confirming the electrical and mechanical

properties of h-BN monolayers and defective BNNTs.[118] BNNSs are most often employed as hydrogen storage materials and as thermally conductive, electrically insulating nanofillers to enhance polymer thermal conductivity. Key features include high mechanical strength, excellent surface adsorption, chemical stability, electrical insulation, and notable gas permeability.[35,117,119] In one study, atomically thin h-BN exhibited wetting visibility comparable to that of graphene.[120]

The large-scale production of high-quality BNNSs, combined with design knowledge and fabrication methods for polymer/BNNS nanocomposites, is crucial for tailoring properties and enabling their widespread applications. Among synthesis routes, bottom–up processes (*e.g.*, arc discharge, CVD) can produce high-grade BNNSs from various boron/nitrogen feedstocks.[121] Top-down approaches are better suited to large-scale production, relying on inexpensive precursors and straightforward exfoliation of bulk BN into nanosheets. Exfoliation methods include mechanical cleavage, liquid-phase exfoliation, and solvothermal-assisted techniques for producing atomically thin h-BNNSs. Although yields are low, mechanical cleavage can produce high-quality monolayer BNNSs from bulk BN.[122] Ball milling[123] and sonication[124] have also been studied for direct exfoliation of bulk BN in liquid media, where BNNs dimensions and defects rely on the applied mechanical energy and duration. For instance, higher milling speeds or prolonged sonication impart greater shear and force on bulk h-BN which produce thinner nanosheets with small lateral sizes and more defects while milder speeds or shorter durations preserve the crystalline integrity and larger flake sizes. Hence, a compromisation could be reached through optimizing the different parameters. High-gravity liquid-phase exfoliation in a rotating packed bed yielded two functionalized BNNS variants: OH-BNNSs *via* polyvinyl alcohol-assisted aqueous exfoliation, and NH_2–OH–BNNSs *via* an ammonium bicarbonate-assisted ball-milling pretreatment followed by rotating packed bed exfoliation.[125] This illustrates how additives can enable simultaneous functionalization of BN nanosheets where polyvinyl alcohol aids the attachment of hydroxyl groups to BN basal planes (OH-BNNSs) and ammonium bicarbonate decomposition releases NH_3 and CO_2 gases during exfoliation that also aid layer delamination and introduce $-NH_2$ and –OH functionalities onto the sheets. As mentioned before, the grafted polar groups prevent restacking and enhance hydrogen-bonding with water and by adjusting the polyvinyl alcohol or NH_4HCO_3 concentrations, one can tune the exfoliation efficiency, nanosheet thickness, and density of functional defects. Another study reported a scalable planetary ball-milling approach with liquid polyethyleneimine to exfoliate pristine BN into monolayer BNNSs at high yield,[126] where the high viscosity of polyethyleneimine played a dual role in the milling process by functioning as milling aid, since it enhance the transfer of shear forces to the bulk material, and providing protective environment for the freshly cleaved nanosheets, since its molecules adsorb onto BN surfaces which suppresses restacking, passivate the surface, prevent aggregation, and limits further uncontrolled fragmentation, ultimately favoring the formation of monolayer BNNs rather than smaller fragments. Teng *et al.* ball-milled h-BN in *N*-methyl-2-pyrrolidone, producing defect-free, few-layer h-BNNSs.[127] As mentioned before, *N*-methyl-2-pyrrolidone's surface energy closely matches that of BN which in milling lubricates interlayer slip, reduce force needed to separate layers, and absorbs milling heat and shock, reducing the lattice strain and producing fewer defects.

Xue *et al.* synthesized gram-scale h-BN nanosheets by annealing a ball-milled $NH_4BF_4/NaBH_4$ precursor under flowing NH_3 (1400 °C, 6 h);[128] The underlying concept of this process is to first ball-mill the precursors into an amorphous precomposite, followed by high-temperature annealing under NH_3 to promote mixing and remove byproducts since the prolonged high temperature allows BN layers to crystallize and grow, while volatile species (BF_3 and H_2) are continuously driven off. In this sense, the milling parameters (which affect precursor homogeneity) and annealing conditions (temperature ramp, hold time, NH_3 flow rate) were the parameters that required fine-tuning. Wang *et al.* reported solvothermal-assisted exfoliation using magnetic stirring and Li^+ to enhance efficiency and produce high-yield h-BNNSs.[129] Li^+ intercalation resembles that of K^+ mentioned earlier, where Li^+ ions are inserted between BN layers under vigorous stirring conditions, weakening the interlayer van der Waals forces and causing lattice expansion and once the mixture is cooled, Li^+ is washed away; This makes Li^+ concentration and the temperature/time profile determine the extent of exfoliation, defects, and residues if Li^+ isn't fully removed.[80] A NaCl-template route, 3–5× more efficient than ball milling/liquid exfoliation, produced >1 g of crystalline, high-purity BNNSs in a single procedure and its hydroxylated BNNSs (OH-BNNSs), at 1 mg mL^{-1}, exhibited excellent water dispersibility and remained stable for >2 days without precipitation.[130] Herein, the method demonstrates how a sacrificial template can dictate 2D morphology where boron and nitrogen precursors are mixed with salts like NaCl, often by spray-drying, to coat the salt crystals and then BN nucleates and grows as a thin layer on the salt surfaceinstead of agglomerating into bulk particles upon high-temperature ammonia pyrolysis and after cooling the salt template is dissolved in water to release BNNs. By varying the salt particle size or heating profile, one can also influence the lateral dimensions of the BNNS (finer salt and rapid heating tend to produce smaller nanosheets with more edge sites, whereas coarser templates yield larger sheets), thus controlling BNNS thickness, lateral size, and defect functionalization *via* simple salt inclusion and removal steps. Surface modification of 2D nanomaterials controls their device integration and tunes properties.[44] Wang *et al.* discussed doping effects on h-BN structure, conductivity, and dielectric properties, and applications as substrates and counter-electrodes in electronics.[47]

Recently, h-BNNSs have proven particularly effective as lubricant additives. This is primarily attributed to weak interlayer shear of the basal planes, tribofilm formation, and mending/polishing effects. Physical and chemical functionalization are commonly employed to improve stability and dispersibility of h-BNNSs in liquid lubricants. Gupta *et al.* evaluated the impact of four distinct dispersants on the stability of h-BNNS in engine oils. At 1 wt% polyisobutylene succinimide, h-BNNSs did not precipitate in engine oil for three weeks,

identifying polyisobutylene succinimide as one of the most effective dispersants.[131] In contrast, other dispersants such as oleic acid exhibited poor dispersion performance.[132]

In one study, OH-BNNSs were synthesized with an 80.1% yield and exhibited dispersibility up to 5 mg mL^{-1}. Beyond their aqueous stability, OH-BNNSs also functioned as green, water-based lubricant nano-additives for metals, effectively reducing friction coefficients and mitigating corrosion by lowering corrosion current density.[133] A ball-milling approach with TA yielded hydrophilic BNNS-TA with 60% yield, ~3.4 μm lateral size, and high-water solubility of 40 mg mL^{-1}; TA, a polyphenol, acted like polyethyleneimine mentioned earlier where it adsorbs onto BN surfaces during milling to prevent restacking and introduce phenolic –OH groups on the exfoliated sheets, increasing its dispersibility in polar matrices, and incorporating this BNNS-TA into epoxy produced thermal-management composites with enhanced mechanical and thermal performance.[134] Beyond thermal management, h-BNNSs combine high mechanical strength, thermal conductivity, electrical insulation, and structural stability. The electronic band structure depends on thickness and interlayer coupling, reflecting quantum confinement effects and strong interlayer interactions. These dynamic properties render 2D BNNSs suitable for a wide range of optoelectronic applications.[135]

In one study, a simple hydrothermal method produced OH-BNNSs (boric acid and arginine as precursors) for uric-acid detection. The as-prepared OH-BNNSs exhibited strong blue fluorescence under UV.[136] Another study produced S-doped and F-doped nanosheets by exfoliating bulk BN, followed by heat treatment.[46] Functionalized BNNSs prepared *via* nitrene cycloaddition exhibited strong adsorption of molecules such as L-cysteine, demonstrating promise for membrane and electrochemical sensing applications.[137]

Recent advances in bottom–up synthesis have enabled the fabrication of large-area single-crystalline 2D BN films *via* CVD on metal foils as evidenced by Wen *et al.*,[138] who used low-pressure CVD on Cu foils to yield continuous monolayer h-BNNSs with areas spanning 4 × 2 cm^2, while maintaining excellent crystallinity, uniformity, and can be transferred intact onto arbitrary substrates as a uniform dielectric coating. Ma *et al.*[139] achieved wafer-scale single-crystalline h-BN by epitaxial CVD on a single Ni(111) crystal, where the aligned h-BN domains on the metal crystal coalesced into continuous monolayer and tri-layer films. These films exhibited a nearly defect-free lattice and were transferred onto SiO_2/Si to serve ultra-clean dielectric layers in MoS_2 transistors, which significantly reduced charge-carrier scattering. Such findings demonstrate that CVD-grown h-BN delivers continuous, highly-ordered, single-crystalline layers in wafer/centimeter-scale that can be directly transferred as insulting sheets with minimal grain boundaries and great structural coherence. Moreover, their large-area provide atomically flat and uniform dielectrics, which enable reproducible performance across the chips, and their strength, high optical transparency, wide band gap (~6 eV), and low defects make them attractive in nanoelectronics and deep-UV photonics.[139] By contrast, BNNSs obtained from top–down exfoliation (*e.g.*, ball milling or ultrasonication of bulk h-BN) are typically smaller and more defective due to harsh exfoliation mechanical/chemical conditions that introduce vacancies, edge defects, or surface functional groups and yield nanosheets with lateral dimensions of <1–5 μm, making their integration into devices rely on processing solutions or manual placement which leads to random orientations, inter-flake junctions and non-uniform coverage.

2.4 Macroscopic BN architectures: fiber assemblies and BN-coated fibers

Beyond the conventional 0D, 1D, and 2D boron nitride nanostructures, recent studies have demonstrated that BN can also be engineered into macroscopic architectures, such as continuous fibers and hybrid core–shells, and these macroscopic configurations retain BN's nanoscale properties (thermal stability, chemical inertness, and electrical insulation) while offering new advantages not attainable with discrete nanosheets or nanotubes alone (mechanical robustness and design flexibility). Thus, opening pathways to functionalities and applications that require both nanoscale performance and macroscopic processability.

One strategy for constructing macroscopic BN architectures is the assembly of 2D BNNSs into continuous fibers. Cheng *et al.*,[140] for instance, applied a radial electric field during spinning of hexagonal BNNSs with polyvinylidene fluoride filaments which enhanced stress transfer, polarized the BNNSs and filaments, and resulted in BNNSs/polyvinylidene fluoride fibers that exhibited a piezoelectric sensitivity six times higher than that of fibers produced without the electric field alignment. This improvement highlights how ordered BN assemblies can impart fibers with great electrochemical response and be applied as highly sensitive sensors capable of detecting subtle mechanical signals. An alternative route for fiber synthesis is to spin the pure BN itself *via* polymer-derived ceramic routes. This was demonstrated by Lee *et al.*[141] who electrospun *N*-methyl polyaminoborane, a boron-rich polymer, and transformed it into continuous low-density h-BN microfibers through ammonia annealing, where those ceramic BN fibers combined the dielectric behavior together with high thermal conductivity while maintaining mechanical integrity, at temperatures that conventional carbon fibers were readily oxidized at.

Another emerging strategy is to conformally coat BNNSs or thin BN layers onto conventional 1D templates to produce core–shell hybrid fibers. In these architectures, a host fiber substrate (such as carbon, ceramic, or optical fiber) is uniformly sheathed in a BN layer to combine BN's properties with the core's mechanicals, making these architectures fundamentally different from intrinsic BNNTs despite pursuing a similar concept (encapsulating 1D forms in a BN environment). On one hand, a BNNT is a self-supporting cylinder (nanometer diameters) composed entirely of BN and exhibits exceptional strength and thermal stability, but their synthesis relies on specialized techniques, such as laser ablation, and yields relatively short tubes which limits their scalability and integration into macroscopic textiles or load-bearing architectures. On the other hand, a BN-coated fiber features a micron-scale core (readily

available fibers) surrounded by a polycrystalline BN shell (tens to hundreds nanometers thick) using solution-based methods or vapor-phase deposition which provides a far more accessible and scalable route and can be integrated into existing composite manufacturing processes. Moreover, the core fiber governs the overall geometry and the mechanical load-bearing-capabilities, while the BN layer extends its role beyond mere protection by also imparting some functionalities. Cheng *et al.*[142] grew a vertically stacked h-BN/graphene heterostructure inside a hollow-core optical fiber to take advantage of BN's insulating and waveguiding properties and tune the fiber's anti-resonant optical modes. This configuration made the BN layer serve as a spacer and dielectric cladding for graphene, enhancing all-optical modulation efficiency by approximately 75%. Elçin *et al.*[143] used a wet-chemical dip-coating and nitridation process to produce uniform h-BN films on carbon fiber tows which exhibited dramatically enhanced oxidation resistance and improved their performance at high temperatures compared to bare carbon fibers and ceramic oxide coatings due to their ability to form viscous B_2O_3 glass at temperatures above 800 °C that effectively self-seals microcracks and blocks oxygen diffusion into the underlying carbon.

Lastly, the BN nanofillers' dimensionality also influences the composite's macroscopic properties. Chen *et al.*[144] demonstrated that 1D BNNTs span across the composite, align under stress, bridge microcracks, and that their elongated fibrous morphology favors early percolation and entanglement within the matrix, which all led to enhanced mechanical strength and thermal conductivity, and more uniform dissipation of stress compared to 2D BNNSs at equivalent loadings, which was also supported by Orikasa *et al.*[145] In contrast, 2D BNNSs interact with the composite over a broad surface area and form an overlapping platelet framework, which is advantageous for withstanding higher compressive forces, and increasing the composite stability and stiffness compared to BNNTs, however, BNNSs' platelet nature and lubricating effect introduce challenges.[145,146] If BNNSs aren't dispersed well or there is weak interfacial bonding, there is a chance for their restacking and agglomeration which leads to the sheets slipping under stress and ineffective load transfer which is why surface functionalization or interfacial modifications are often employed to improve BNNSs-polymer adhesion and mitigate this slippage. These insights highlight that different BN dimensionalities offer distinct but complementary advantages and open venues for their combination. As a result, Wu *et al.*[147] have recently designed hybrid 1D and 2D BN filler frameworks to combine uniform stress deflection, thermal and mechanical percolation of BNNTs with the maximal interfacial contact and stiffness of BNNSs.

3 Applications of boron nitride nanomaterials

The recognition that BN allotropes are architecturally versatile, comparable to carbon forms (fullerenes, graphene, nanotubes), has renewed their prominence in contemporary materials science. BN materials are attractive owing to their dispersion stability, low density, oxidation/thermal resistance, strong adsorption, and optical transparency. Practical applications of BN systems require complex synthesis, processing, and nano-design strategies that impart unique structural and functional characteristics. Such approaches enable performance in hydrogen storage and water purification.[148,149] Three-dimensional BN nanostructures have been widely documented for their efficacy in water treatment and as antibacterial agents. BN-based composites can be engineered for low microwave loss and radar transparency, enabling radome structures (which protect RF systems while transmitting electromagnetic signals) with high strength, environmental tolerance, and reduced weight.[150]

h-BN serves as an excellent substrate for semiconductors and metal-oxide-semiconductor field-effect transistors owing to its intrinsic thermal and dielectric properties. Reducing BN to monolayers or nanoscale lateral dimensions reveals properties such as piezoelectricity, enabling sensors and actuators concepts. Reported applications also include magnetic/semiconducting devices,[151] photodetectors and optoelectronics,[87,152] photocatalysis,[13,153] energy storage,[154] quantum emitters,[155,156] aerospace structures,[157] surface-enhanced Raman spectroscopy substrates,[119] and polymer-matrix gas-barrier composites.[158] Li *et al.* lately reviewed the environmental applications of h-BN and outlined future perspectives.[36]

Ongoing research highlights promising biomedical applications of BN nanomaterials, including cancer therapy and wound healing. Dean *et al.* reported the biocompatibility/low toxicity, as well as the thermal/chemical stability (up to ~800 °C in air) of nano-BN, which is comparable to that of SiO_2, supporting its applications in tissue engineering, biosensing, and drug delivery.[24,159] Many state-of-the-art BN nanostructure-based drug delivery systems have been developed with improved solubility and physiological compatibility.[130]

Leveraging thermal conductivity, chemical inertness, and mechanical strength, nanostructured BN can mitigate short circuits, dendrite growth, and other failure modes in conventional batteries, improving safety and cycle life.[160] An h-BN-based nanocomposite ($Li_4Ti_5O_{12}$/rGO/h-BN) used as an electrode showed lower resistance, enhanced ion transport/electron mobility, and higher Li^+ retention.[161] Studies showed that functionalized BN nanomaterials interact with $TFSI^-$ to enhance Li^+ mobility and transference number in ion-gel electrolytes; a $LiFePO_4$|Li cell employing an amine-functionalized BNNS gel electrolyte exhibited uniform Li deposition and improved battery performance.[162–164]

BN enhances the lubricating qualities of ceramics, metals, rubber, and plastics, while BN nanosheets improve paints and coatings by increasing wear resistance, interfacial bonding, anti-corrosion behavior, hydrophobicity, and oxidation resistance. Consumer uses (*e.g.*, pencil lead, paint lubricants, cosmetics, dental cements) also benefit from BN's enhanced softness and stability.[165] This review tries to highlight and cover some of the widest application subsets of the numerous potential BN nanomaterial applications.

3.1 Analytical chemistry applications

3.1.1 Electrochemical sensors. Electrochemical sensors are receiving considerable attention owing to advances in early detection and monitoring techniques. Extensive research has focused on developing contemporary electrode materials with enhanced physicochemical properties to improve electrochemical performance for continuous monitoring.[166] Hexagonal BN (h-BN) shows promise as an electrochemical sensing material due to its unique structural and electrochemical characteristics. Beyond these attributes, the morphology of BN strongly influences its electrochemical performance. Since BN is intrinsically insulating, its role in electrochemical systems is often as a co-reactant, structural support, or heterostructure component, rather than as a standalone conductor. Two-dimensional BN nanosheets (BNNSs) receive the greatest attention for electrode modification in both fundamental studies and practical applications. Heterostructures integrating the conductive/semiconducting carbon nanostructures with insulating BNNSs enable the fabrication of electronic devices, field-effect transistors, and tunneling architectures.

Additionally, BNNSs' chemical inertness provides corrosion resistance, and their smooth surfaces enhance device quality and performance.[167] Multiple reviews have highlighted advances in h-BN sensor fabrication for biological, gas, pH, optical, and electrochemical applications, including electrochemical sensing with 2D h-BNNSs.[168,169] For biological samples, electrochemical detection offers on-site analysis, low cost, simplicity, rapid response, compact instrumentation, and microscale detection capability. Although techniques such as enzyme-linked immunosorbent assay, thermal sensors, high-performance liquid chromatography (HPLC), liquid chromatography-mass spectrometry, microemulsion electrokinetic chromatography, and fluorescence spectroscopy are widely used, electrochemical sensors offer distinct advantages in sensitivity, cost, and practicality.[170]

Electrochemiluminescence (ECL) is light emission from electrochemically generated excited states under an applied potential. An ECL-based DNA sensor for BRAF gene detection was developed using sulfur-regulated BNQDs.[171] Wang *et al.* employed BNQDs as co-reactants in ECL biosensors for concanavalin A, achieving a tenfold ECL intensity increase, which demonstrates the utility of BNQDs as luminophore enhancers.[172] Kamyabi *et al.* developed a high-performance ECL sensor for tribenuron using BNQDs as co-reactants in a Ru/AgNPs/GO/glassy carbon electrode (GCE). Non-toxic BNQDs outperformed tripropylamine as a co-reactant in enhancing luminophore signals, and tribenuron-methyl further amplified the ECL response.[173] Another ECL sensor for diazinon employed a ternary nanocomposite film GO/AgNPs/$(Ru(bpy)_3)^{2+}$ on a GCE, with BNQDs as co-reactants to enhance ECL signal; diazinon was detected *via* pronounced ECL quenching from diazinon-BNQD binding and radical consumption.[174] Additionally, Qin *et al.* constructed a label-free ECL immunosensor for α-fetoprotein using a rGO@Au@Ru-SiO_2 nanocomposite; BNQDs acted as co-reactants, catalyzing oxidation, lowering the oxidation potential, and amplifying the ECL response.[175]

Beyond ECL platforms, BN-based composites support voltametric and amperometric sensing of diverse analytes. For nitrofurantoin, a compound associated with toxicity at high doses, a non-invasive, highly sensitive, and selective electrochemical sensor was developed using an α-Fe_2O_3/h-BN nanocomposite; the sensor was simple, rapid, and inexpensive.[176] A BNNS-doped graphene film (top–down prepared) functioned as a hybrid binary composite for electrochemical nicotine detection.[177] A yttrium-oxide/BN (YO/BN) nanocomposite prepared sono-chemically was used for dopamine detection.[178] Halloysite nanotubes (HNTs) are also gaining attention as electrochemical sensors due to their high porosity, large specific surface area, low cost, and biocompatibility.[179] A h-BN/HNT nanocomposite sensor demonstrated exceptional selectivity for furazolidone, an antibacterial and antiprotozoal medication, even with high levels of interferents.[180] Another Bi_2O_3/h-BN nanocomposite sensor enabled efficient flutamide detection in ambient samples.[181] AuNPs combined with 2D-h-BN nanosheets were utilized for the detection of diethylstilbestrol.[182] Another sensor combining 2D-h-BN nanosheets with Fe@AuNP core–shell materials enabled the detection of cypermethrin pesticide in wastewater.[183]

3.1.2 Fluorescence spectroscopy and chemiluminescence. Spectrofluorimetry remains a cornerstone in trace analysis due to its high sensitivity, simple optics, and facile signal readout. Boron nitride (BN) nanomaterials, ranging from few-layer hexagonal nanosheets (h-BNNSs) to BN quantum dots (BNQDs), are emerging as highly attractive platforms for spectrofluorimetric sensing. They can serve as insulating, chemically inert spacers that preserve fluorescence near quenchers or electrodes; as universal nano-quenchers for biorecognition; and as emissive probes *via* defect/dopant engineering. Unlike conductive 2D quenchers such as graphene oxide, h-BN's insulating character allows switchable functionality: serving as a kinetic/affinity-tuned quencher in nucleic acid assays, an emissive scaffold after controlled functionalization, and an atomically precise dielectric spacer that either suppresses NRET or enables MEF. Their wide band gap, optical transparency, and chemical robustness support this versatility, enabling reproducible and biocompatible sensor platforms.[184,185]

Exfoliated h-BNNSs effectively quench dye-labeled single-stranded DNA (ssDNA) probes *via* π–π interactions and electron transfer but interact weakly with the rigid DNA–RNA duplexes that form after hybridization. Leveraging this property, Li *et al.* designed a signal-on fluorescence assay in which a complementary microRNA binds to the ssDNA probe to form a DNA–RNA duplex. This duplex weakens probe adsorption on h-BNNSs, leading to desorption and fluorescence recovery. This platform achieved a 2.39 nM detection limit (DL) with single-base mismatch selectivity, demonstrating how duplex-induced desorption can be exploited for highly sensitive and selective microRNA detection.[186]

Beyond physical quenching, BN nanoplatforms are now being engineered with catalytic functionalities to enhance robustness and broaden applicability. Nemati and Hosseini functionalized BNNSs with Ce, producing peroxidase-like Ce-BNNSs that oxidized *o*-phenylenediamine into fluorescent

oxOPD (λ_{em} ~562 nm); oxOPD quenches intrinsic Ce-BNNS emission (~447 nm) *via* an inner-filter effect, enabling ratiometric F_{562}/F_{447} with DL = 50 pM.[187] Similarly, hydrothermally synthesized OH-BNNSs display bright blue emission (λ_{em} ~360 nm at λ_{ex} = 300 nm), selectively quenched by uric acid, achieving DL = 16 nM with accurate recoveries in urine and serum.[136] Tungsten(W)-doped BN nanosheets further expand this concept: combining their strong intrinsic fluorescence with selective W–thiol interactions, enabled the detection of the cancer marker cysteamine in biofluids with DL = 93.6 pM.[188]

Furthermore, the visible emissions of BNQDs often originate from defects or dopants, which can be deliberately engineered to create ratiometric probes. Wang *et al.* reported BNQDs that, upon Hg^{2+} binding (λ_{ex} = 280 nm), exhibited simultaneous quenching of the blue emission (~461 nm) and the emergence of a yellow-green band (~560 nm), yielding a ratiometric signal with DL = 0.7 nM. When incorporated into paper test strips with smartphone readout, this system achieved field-level detection (~1.9 nM), underscoring its portability for point-of-care monitoring.[189] Extending upon BNQD environmental applications, Peng *et al.* reported a green-synthesized BNQD turn-off probe for 2,4,6-trinitrophenol, achieving DL = 0.14 μM with high selectivity over related nitroaromatics and reliable recoveries in natural waters.[190] Shokri *et al.* extended BN-derived probes beyond fluorescence to chemiluminescence (CL), designing a CL sensor for trifluralin. In this system, a BNQD–Co^{2+} complex catalyzed the H_2O_2-mediated oxidation of pyrogallol, amplifying luminescence, with trifluralin detected through its quenching effect on the enhanced signal.[191]

Recent work has expanded BN-based luminescent platforms beyond single-function probes by strategically pairing BNQDs and BN dots. In such hybrids, BNQDs provide excitation-dependent emission, while non-fluorescent BN dots act as inert dye carriers, suppressing quenching and thereby enabling high-brightness hybrid probes. This concept of pairing emissive and insulating BN structures extends to applications where BN's wide band gap and dielectric properties are leveraged to control energy transfer. For instance, atomically thin h-BN serves as an ideal dielectric spacer to regulate NRET and support MEF. Yang *et al.* demonstrated this by stacking h-BN with graphene to precisely tune dye-graphene separation, observing fluorescence recovery that scaled with distance ($\propto d^{-4}$), with ~20 nm h-BN restoring emission nearly to the SiO_2/Si baseline.[185] In parallel, Gan *et al.* employed h-BN as a pinhole-free MEF spacer over Ag nanoparticles, achieving fluorescence enhancement factors ~95 ± 5, sensitivity down to ~10^{-8} M, and excellent thermal and chemical reusability.[184] Together, these studies underscore how BN nanomaterials, whether as emissive QDs, inert Scarriers, or atomic spacers, offer versatile platforms for constructing advanced, energy-transfer-controlled spectrofluorimetric systems.

The evolution from simple 'turn-off' assays to ratiometric, catalytic, MEF-assisted, and hybrid formats highlights the versatility of BN nanomaterials in spectrofluorimetry. Current challenges lie in controlling BNQD defect chemistry to achieve standardized emission, developing reproducible functionalization without compromising photophysics, and translating proof-of-concept assays into multiplexed, matrix-tolerant on-chip platforms. Nonetheless, the integration of ratiometric readouts, portable formats (*e.g.*, paper/smartphone systems), and hybrid devices positions BN-based spectrofluorimetry as a promising frontier for sensitive, selective, and field-deployable biomedical and environmental applications.

3.1.3 Adsorption and chromatographic separations. Beyond its applications in ECL, CL, and spectrofluorimetry, BN also exhibits strong adsorption capacity. Adsorption stands out among separation/extraction techniques for its simplicity, low solvent use, and high efficiency. Effective adsorbents require large specific surface area and mechanical strength to provide abundant adsorption sites and long-term stability. BN nanomaterials fulfill these requirements, underscoring their potential as adsorbent substrates. BN structures have also demonstrated strong adsorption capacity for mitigating water contamination. Examples of targeted organic and inorganic water contaminants include dyes, heavy metals, and anions (such as phosphate, sulfate, nitrate, and chloride); elevated levels pose serious environmental and health risks. BN-based adsorbents have shown comparable or superior performance to most conventional water-treatment adsorbents.[192] Numerous techniques such as solvent extraction, electrodeposition, precipitation, and adsorption have been explored for uranium-lanthanide separation, with adsorption proving particularly effective due to the properties outlined above. Porous BN can uptake up to ~3300 wt% of liquids/contaminants, demonstrating high uptake, and shows excellent cycling stability, extending operational lifetime.[167]

The lightweight, layered, high surface area structure of h-BN provides numerous active sites for hydrogen adsorption especially that they also offer mechanical robustness, chemical inertness, and stable adsorption–desorption cycling. Additionally, their graphene-like framework (BNNTs' analogy to CNTs) can store hydrogen primarily through physisorption and the intrinsic polarity of the B–N bond and the presence of defects introduce slightly stronger binding interactions.[193] Li *et al.* reported BN whiskers with 1687 $m^2 g^{-1}$ surface area that achieved fully reversible adsorption and 5.6 wt% hydrogen uptakes at room temperature under 3 MPa.[148] To further enhance hydrogen storage performance and highlight how subtle changes in BN chemistry can tune hydrogen-surface interactions without sacrificing reversibility, chemical modification strategies have been developed. For instance, metal decoration of BN surfaces can increase hydrogen binding through polarization effects and Kubas-type interactions[194] and partial substitution of BN with carbon to form boron-carbon-nitride introduces additional electronic states that strengthen hydrogen adsorption for metal-free storage capacities.[195] Furthermore, combining BN with secondary components has also proven effective. In one study, h-BN particles synthesized hydrothermally (200 °C, 24 h) were deposited onto CNT surfaces, forming an h-BN/CNT heterostructure and then dip-coated onto porous Ni foam in <15 minutes. Hydrogen storage capacity was evaluated using electrochemical impedance spectroscopy, cyclic voltammetry, and galvanostatic charge–discharge in 6 M KOH at room temperature which showed that h-BN decoration of CNTs enhanced hydrogen

adsorption capacity, attributed to morphology transition from flake to spherical which increased surface-active sites.[196]

Another study investigated CO_2 absorption in methyldiethanolamine (MDEA) solutions using 2D h-BNNSs. The effects of MDEA concentration and h-BNN loading on CO_2 absorption were systematically evaluated. CO_2 absorption increased with h-BNNSs loading up to 0.025 wt% but declined at higher loadings. The maximum enhancement observed was 3.98% in 5 wt% MDEA solution containing 0.025 wt% h-BNNs; higher MDEA concentrations diminished the enhancement.[197]

Liu *et al.* employed DFT simulations to investigate the adsorptive desulfurization mechanisms on defective h-BNNSs doped with single Ag atoms. The enhanced adsorption of thiophenic compounds was driven by strong S–Ag bonding, supported by π–π interactions and electrostatic contributions. These findings provide insights into the rational design of selective, high-performance single-atom adsorbents for desulfurization applications.[198] Liu *et al.* reported Cu-doped BNNS (Cu-BNNS) as solid-phase extraction (SPE) adsorbents for rhodamine B quantification in food, achieving recoveries of 89.8–95.4% under optimized conditions.[199] BN-based adsorbents have also been applied in SPE workflows for the extraction of pesticides,[200] herbicides,[201] and polychlorinated biphenyls[202] from water samples.

Beyond batch adsorption, BN's interfacial chemistry also underpins dynamic separations in chromatography. BN has been engineered as a chromatographic stationary phase, exploiting its high surface area, thermal stability, and tunable interfacial chemistry to enable selective separations. In HPLC, pristine BNNTs were non-covalently immobilized as ultrathin coatings on monolithic silica or amino-silica particulates, producing stable phases with enhanced retention and efficiency while preserving nanotube integrity. The BNNT-coated monolith resolved phenol derivatives, alkylbenzenes, and steroidal doping agents under both isocratic and gradient modes, with good repeatability and column durability. This highlights the role of hydrophobic and π-interactions at the BNNT interface.[203] Complementarily, the BNNT-coated particulate enabled quantitative analysis of β-cyclodextrin host–guest complexation for terpene drug surrogates; the measured formation constants matched literature values. The retention trends in MeOH/H_2O systems also demonstrated the direct BNNT contribution to molecular recognition.[204] Extending to gas chromatography, statically coated h-BN capillaries exhibited moderate polarity (McReynolds index ∼136), preferential retention of polycyclic aromatic hydrocarbons over phthalate esters, strong selectivity for halogenated analytes, and high resolution of structural and positional isomers, with robust repeatability (run-to-run RSD 0.03–0.07%) and thermal stability up to ∼260 °C. These behaviors were attributed to the ionic B–N lattice, temperature-dependent surface corrugations, and π/halogen-bonding interactions, which distinguish h-BN phases from conventional polysiloxane or g-C_3N_4 stationary phases.[205]

3.2 Material science

3.2.1 Biomedical applications. Since the advent of nanomedicine, numerous polymeric and non-polymeric nanomaterials have been investigated as potential drug carriers. An effective carrier must deliver and release drugs within target cells while maintaining flexibility, stability, and low toxicity under physiological conditions.[206] As a result, h-BN, noted for its low toxicity, holds strong potential for functional drug delivery systems. Porous BN can be engineered with high specific surface area to enhance drug-carrying capacity, although surface polarity and potential hydrogen-bonding in sp^2 B–N frameworks may impact biocompatibility. Consequently, surface modification and precise size control are necessary to mitigate these limitations. One study found that heteroatom doping (*e.g.*, with sulfur or fluorine) significantly modulated h-BN's drug uptake and release behavior, enabling intracellular retention without adverse effects.[46] Boron nitride nanoparticles (BNNPs), especially BN nanospheres, have also been investigated as nano-drug delivery vehicles for chemotherapeutic drugs.[207] BN nanospheres (20–200 nm) are attractive carriers due to their biocompatibility and ability to interact with hydrophobic drug sites.[30] Zhang *et al.* (2013) investigated chitosan-coated BN nanospheres as carriers for CpG oligonucleotides, demonstrating enhanced delivery and potential use for immunomodulatory vaccines, allergy treatments, and cancer therapies.[208] Feng *et al.* (2016) developed a folic-acid (FA)-functionalized BN nanosphere drug delivery system, in which FA was conjugated to BN nanospheres *via* esterification.[209] Subsequent work adopted a three-step protocol involving FA pre-activation to facilitate FA coupling to BN carriers. AgNPs were first deposited on BN carrier, then modified with L-cysteine to introduce terminal –NH_2 groups, yielding FA-Cyst-Ag/BN.[210] For comparison, drug adsorption/release on nanotube surfaces was found to depend on diameter and composition, with silicon carbide nanotubes showing the lowest release efficiency.[211]

In light of the unique structure and properties of h-BN, it is being investigated for disease diagnosis and therapy. In diagnostics, Kumar *et al.* leveraged the intrinsic blue emission of BN nanoflakes to demonstrate biocompatible fluorescence imaging, supporting BN's suitability for bioassays.[212] Beyond diagnostics, BN nanocrystals have shown potential in boron neutron capture therapy for selective tumor ablation, as well as thermal ablation and neutron sensing.[213] h-BN-Au nanohybrids, produced by physical/chemical exfoliation of h-BN with Au, did not impair cellular metabolism, reduced proliferation of MCF-7 cancer cells relative to L929 normal cells, and altered lysosomal activity in both malignant and normal cells.[214] In another study for targeted tumor therapy, a biomimetic nanoplatform (CM@BN/DOX; cell-membrane-coated BNNPs loaded with doxorubicin) was developed.[215] Samarium-doped BNNTs (Sm-BNNTs) were synthesized by thermal CVD (samarium oxide, 1150 °C, NH_3/N_2 gas mixture). Subsequent reactor activation generated ^{152}Sm radioisotopes within BNNTs; characterization confirmed successful doping, indicating therapeutic potential.[216]

Additionally, nanomedicine materials must exhibit superior chemical and physical properties while ensuring that their degradation products do not compromise cell viability. BNNPs have demonstrated favorable biological activity and have been explored as nano-therapeutics against a range of infections. A

poly(hydroxyethyl methacrylate) (pHEMA)/functionalized-BNNS composite showed no cytotoxicity and exhibited antibacterial activity against *S. aureus* and *E. coli*; the bionanocomposite outperformed pHEMA alone, with greater efficacy against *E. coli*.[217]

Moreover, boron-based materials have also enabled new strategies for tissue engineering. Incorporating ultrasonic-induced piezoelectric components (BNNTs and barium titanate ($BaTiO_3$)) into poly(ε-caprolactone) to mimic bone tissue piezoelectricity increased osteogenesis-related activities.[218] Cadmium-doped BN (Cd-BN) biomaterials for bone regeneration showed encouraging cytocompatibility and potential biomedical applicability at higher Cd ratios.[219] Nonetheless, given cadmium's systemic toxicity, *in vivo* evaluation with attention to dose-limiting effects is essential. Hyperbranched polyglycerol-functionalized-BNNSs yielded a BNNSs/gelatin nanocomposite that enhanced adipose stem-cell adhesion, proliferation, and longevity *in vitro*.[220]

Kakarla and Kong reviewed the role of BNNTs in biocompatibility, emphasizing their impact on cell survival, proliferation, therapeutic outcomes, and genotoxicity, all critical for biomedical applications.[221] Cell-derived biomimetic carriers exhibit strong targeting ability, prolonged circulation, and excellent biocompatibility. To support future biomedical translation, a BN@RBCM (red blood cell membrane-coated BN) composite was developed and evaluated; intravenous administration showed no significant acute or subacute toxicity.[222]

3.2.2 Aerospace materials and radiation shielding. Radiation shielding is crucial owing to the extensive use of nuclear sources in power generation, the space industry, and nuclear medicine. In recent years, research has focused on maximizing shielding efficiency while maintaining mechanical durability. Radiation from protons and neutrons, especially secondary neutrons generated by nuclear collisions with high atomic number materials (Z), can cause severe damage. Although not the primary source, neutron radiation can also arise from solar particle events or interactions between spacecraft structures and galactic cosmic rays. Interactions between shielding materials and secondary neutrons can induce scattering, activation, and material damage. Despite being pivotal to science and engineering, space exploration faces significant challenges in mitigating hazardous radiation, which has traditionally necessitated the use of heavy shielding materials in spacecraft. More recently, lightweight and multipurpose shielding materials have become increasingly attractive, particularly those incorporating low-atomic-number elements (*e.g.*, hydrogen) owing to superior attenuation and minimal secondary neutron production.

Hydrogen-containing BN compounds have demonstrated effective shielding against galactic cosmic rays and solar particle events at NASA's Langley Research Center.[223] BN-polymer composites have also been widely studied for neutron shielding. Building on this trend, BN materials, including BNNPs and BNNTs, have become attractive for aerospace applications due to their exceptional thermal and mechanical robustness and neutron-shielding capability. BN's neutron shielding primarily arises from thermal-neutron capture by ^{10}B, affording substantial protection. BN fillers are typically incorporated into polymer composites to enhance both mechanical strength and shielding performance. Shielding performance can be further improved by introducing hydrogen into BNNTs (bonding to lattice sites or occupying vacancies). DFT calculations on double-walled BNNTs (DW-BNNTs) showed that defective armchair tubes suffered larger Young's modulus reductions (5–25%) than zigzag tubes (3–15%), indicating zigzag DW-BNNTs are more mechanically resilient to radiation-induced defects.[224] Chen *et al.* developed a dual-layer h-BN/Al_2O_3 coating for space solar-thermal shielding, integrating radiative cooling with asymmetric thermal transmission. In-plane alignment of h-BN flakes in the top coating layer produced highly anisotropic heat transfer.[225]

Polymer reinforcement with nanoparticles has been shown to improve the radiation-shielding efficiency of nanocomposites. A few fillers additionally impart multifunctional benefits, including improved thermal conductivity, electrical conductivity, and flexural strength. Multilayer configurations increase the likelihood that incoming radiation will be scattered and absorbed by the shield. Incorporating reinforcing fillers into composites generates synergistic mechanical properties unattainable from the individual constituents alone. Fiber-reinforced polymer composites are widely used across various industries, particularly in the aerospace sector. Epoxy resins are the most popular polymer matrices, offering strong mechanical performance, design flexibility, and chemical and electrical resistance. For aerospace applications, polymer composites incorporating BNNPs represent promising options for multifunctional structural materials.[226] In one study, BNNPs functionalized with 3-aminopropyltriethoxysilane (chemical method) or cetyltrimethylammonium bromide (physical method) showed markedly improved dispersion and interfacial compatibility in epoxy matrices. The resulting glass fiber-reinforced composite laminates exhibited enhanced tensile and flexural properties, as well as improved thermal conductivity, while also enhancing radiation-shielding performance. These findings underscore the feasibility of BNNP-enhanced prepregs as a novel and industrially viable approach for manufacturing advanced aerospace structural materials.[227] In a separate instance, a hybrid nanocomposite incorporating 0.5 wt% graphene nanoplatelets and 0.5 wt% h-BN into an aerospace-grade epoxy exhibited substantial multifunctional enhancements, including a 108-fold increase in electrical conductivity, a 69% improvement in flexural strength, and a 7% increase in thermal conductivity compared to neat epoxy. These synergistic effects highlight the potential of GNP/h-BN-tailored epoxies to meet the electrical and thermal management requirements of lightweight avionics chassis, informing the design of advanced thermal interface materials with engineered electrical properties.[228]

Polyethylene/h-BN (PE/h-BN) composites, owing to their flexibility, affordability, and processability, present promising candidates for high-efficiency radiation shielding. Shang *et al.*[229] fabricated multilayer PE films with alternating high-density PE/h-BN (HDPE/h-BN) and low-density PE, in which h-BN platelets are highly oriented in-plane *via* a two-step hot-

pressing process. Neutron shielding performance of multilayer PE/h-BN composites varies with varying h-BN concentrations. Owing to their high hydrogen content, PE films reduced the transmission ratio (I/I_0) by ~50%. Both the linear attenuation coefficient (μ) and mass attenuation coefficient (μ/ρ) increase with higher h-BN content. At equal h-BN loading, the multilayer architecture exhibits higher μ and μ/ρ than randomly structured counterparts. At 30 wt% h-BN, I/I_0 reaches ~4.2% for the multilayer films *versus* ~15.0% for random, indicating markedly superior attenuation. The study compares random (μ/ρ_r) *versus* multilayer (μ/ρ_m); the relative enhancement is defined as $\Delta(\mu/\rho) = (\mu/\rho_m - \mu/\rho_r)/(\mu/\rho_r)$. $\Delta(\mu/\rho)$ was small at low filler contents but was raised to ~41.4% at 30 wt%, consistent with limited multilayer influence at low loading and clear benefits at higher loading.

3.2.3 Thermally conductive electrically insulating fillers and energy applications. Demand for thermally conductive yet electrically insulating composites is rising as power densities in batteries, supercapacitors, and 5G electronics increase because excessive heat accumulation compromises performance, safety, and lifetime.[230] Thermal conductivity (TC) in solids arises from phonon transport (and from electrons in conductors); in composites, filler–matrix interfaces add thermal resistance. Consequently, TC of different materials varies with morphology, crystal structure, and carrier density, which govern phonon/electron transport. For instance, isotropic materials conduct uniformly, whereas anisotropic materials exhibit direction-dependent TC. In any material, structural defects introduce heterogeneity, causing particles to vibrate at different frequencies and enhancing phonon scattering, which ultimately reduces TC. In polymers, the amorphous packing hinders phonon transport, yielding intrinsically insulating behavior. As a result, considerable effort has focused on enhancing polymer TC using fillers such as carbon fibers, Al_2O_3, and high TC graphene. Yet, balancing high TC with strong dielectric insulation and low interfacial thermal resistance remains challenging. h-BN exhibits high in-plane TC (~400 W m^{-1} K^{-1}, comparable to metals) while remaining electrically insulating, which enables efficient heat dissipation without the risk of electrical shorting and encourages their study as polymer fillers. Theoretical studies indicate that atomically thin 2D BN, when used as an interlayer/dielectric spacer, can mitigate interfacial phonon scattering and lower thermal boundary resistance; when oriented into continuous pathways, it enhances effective thermal transport in layered composites due to its high-volume resistivity (10^{13}–10^{15} Ω cm) while preserving electrical insulation. Introducing micrometer-scale BNNS enhances polymers' TC. In contrast, carbon nanotubes often exhibit weaker adhesion than BN nanosheets due to their high surface tension and interfacial thermal resistance with polymer matrices.[231–235] In rechargeable battery cells, BN is widely used as a protective and performance-enhancing additive. From the protection aspect, coating separators with h-BN creates a thermal and mechanical barrier that stabilizes lithium metal anodes and mitigates dendrite penetration, while the performance aspect arises from increasing Li^+ conductivity and mobility due to BN's ability to interact with anions and form a more robust conduction network. Moreover, BN-loaded polymer separators and coatings help redistribute the localized heat during abnormal operating conditions and serve as heat spreaders that remove waste heat while maintaining electrical isolation between components in power electronics and LED modules.[236,237] Unlike conventional separators, which are difficult to make thin without compromising strength, BN nanomaterials can form thin membranes alongside providing excellent dielectric strength and mechanical resilience, which makes them also used as separators in supercapacitors.[193,238] These properties are valuable in emerging energy technologies such as 5G base stations, inverters, electric vehicle battery packs and fast-charging systems, where BN-filled thermal pads and coatings help eliminate hotspots, stabilize temperature gradients across cells, and operate under high heat flux while preserving electrical insulation.

Hybrid materials, such as BN-filled epoxy hybrids, combine high TC with electrical insulation and are widely used for electronic thermal management owing to their simple fabrication. Numerous techniques, including vacuum filtration, hot pressing, electrospinning, and ice-templated freeze casting, have been employed to enhance polymer TC with BNNS-based composites. Furthermore, filling polymer gaps with BN nanostructures yields white or transparent composites that are highly thermally conductive yet electrically insulating.[239] Thus, 2D BNNSs enable polymer blends with exceptionally efficient heat dissipation. For instance, the thermal conductivity of hot-pressed PDMS/BNNS composites reached 1.12 W m^{-1} K^{-1} at 25 vol% BNNS loading.[240] In another experiment, Jang *et al.* fabricated an e-BN/BN/epoxy composite that contained 50 wt% h-BN flakes, corresponding to 33 vol% of the total composite. The e-BN/BN/epoxy composite achieved a through-plane TC of 4.27 W m^{-1} K^{-1}, ~3.7× higher than the BN/epoxy composite (1.17 W m^{-1} K^{-1}).[27] Another laminated BNNS/ethylene-vinyl acetate (EVA) copolymer film achieved an in-plane TC of 13.2 W m^{-1} K^{-1} at 50 wt% BNNS. Additionally, oxygen-containing functional groups on BNNSs improved interfacial coupling with the EVA matrix and reduced phonon scattering.[241]. (Polyimide/rGO)@BNNS composites showed TC of 3.98 W m^{-1} K^{-1} *versus* 0.31 W m^{-1} K^{-1} for neat polyimide and delivered excellent heat dissipation when tried as a thermal interface material in LED bulbs.[242] A further superior in-plane TC of 19.13 W m^{-1} K^{-1} was achieved by the multilayer gradient BNNS/aramid nanofiber films.[243] Using a precipitation method followed by hot pressing, hBN/thermoplastic polyurethane (TPU) composite films were fabricated with filler loadings up to 95 wt% while retaining flexibility. At this loading, the films achieved in-plane TC of 50.3 W m^{-1} K^{-1}, corresponding to a 264-fold enhancement over neat TPU. Due to these superior thermal transport properties, the hBN/TPU films were utilized as LED heat spreaders, reducing operating temperature by ~40 °C.[244] Notably, Niu *et al.* has recently reviewed critical strategies for BN/polymer composites to achieve ultrahigh out-of-plane TC.[245]

Beyond solid composites, the high thermal conductivity of BNNPs has also been utilized in nanofluids, where their dispersion in conventional heat-transfer fluids can significantly

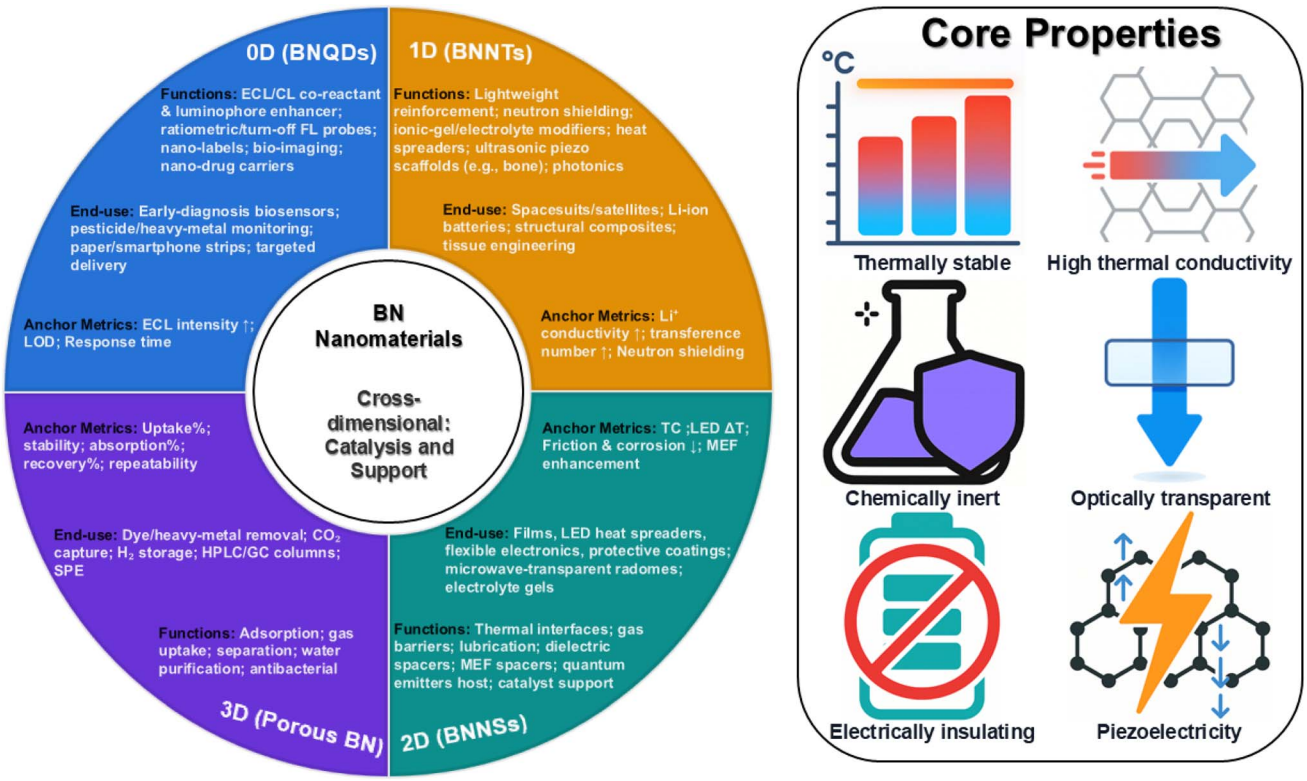

Fig. 4 Summary diagram linking BN properties, functionalities and application domains across different dimensions.

enhance TC and overall heat transport efficiency. Such nanofluids benefit heat exchangers that require rapid cooling or heating, as well as advanced thermal management systems.[246,247]

3.3 Catalysis: metal-free BN and BN as catalyst support

Integrating multiple functional properties within a single catalyst can yield synergistic gains in activity and selectivity. Boron-based catalysts play essential roles in diverse synthetic chemistry reactions, including oxidation, reduction, hydrogenation, dehydrogenation, isomerization, and polymerization. Surface functionalization and atomic doping significantly enhance h-BN catalytic reactivity, establishing it as a promising metal-free catalyst.[246,248] Studies have demonstrated that h-BN functions effectively as a metal-free catalyst in nitrogen reduction, aerobic oxidative desulfurization,[249] dehydrogenation,[250] and hydrochlorination.[251] The catalytic activity of h-BN is commonly attributed to edge B–OH/Lewis-acid B sites, B_xO_y species (*e.g.*, B_2O_3-like, often generated by oxidative pretreatment), adjacent Lewis acid–base pairs (B as acid, N as base), and edge-localized radical species. Additionally, boron atoms at unsaturated edges and defect-rich BNNS surfaces further contribute to reactivity.[252,253]

Recent studies have highlighted the remarkable catalytic performance of boron-containing materials, particularly h-BN in oxidative dehydrogenation of alkanes (*e.g.*, propane to propylene), driven by surface-initiated radical intermediates that subsequently propagate in the gas phase. 3D-printed h-BN monoliths delivered higher propylene/ethylene formation rate ratios and greater olefin selectivity than conventional packed beds of h-BN pellets, underscoring 3D architectural advantages.[254]

An organized BN-like floral catalyst, composed of ~50 nm-long nanofibers, was fabricated using a self-modification method coupled with *in situ* self-assembly. BN-like flowers with low B–O species content exhibited over threefold higher photocatalytic CO_2-to-CO reduction rates than those with high B–O variants, as low B–O levels favor rapid charge transfer and *CO desorption. Various materials, including transition metal dichalcogenides and 2D and layered nanomaterials, have been explored for CO_2 photoconversion. These materials offer high chemical tunability and strong catalytic activity. Moreover, introducing heteroatoms (C, O, P) into BN or forming BCN alloys tunes its band gap and band positions, granting BN-based catalysts the ability to absorb light and participate in photocatalytic water splitting and CO_2 reduction.[255]

Metal-free BN-based catalysts also show promise for advancing solar fuel production.[256]

In nonmetallic BN, polar B–N bonds with a large electronegativity difference, together with defect or heteroatom-doped sites, create adjacent Lewis acid–base pairs that mediate adsorption/activation and charge-transfer steps during CO_2 reduction. BN-based photocatalysts can contribute to CO_2 mitigation *via* solar-driven reduction pathways, thereby helping to mitigate global warming. Chen *et al.* comprehensively reviewed as-prepared h-BN-based catalyst libraries,

Table 1 Consolidated summary of up-to-date review of synthesis methods for BN nanomaterials and their core applications

Approach	Method	Precursors/feedstocks	Dimensionality	Functionalized/dopant	Application
Top-down	Liquid exfoliation → solvothermal (Sealed autoclave)[73]	Bulk h-BN; solvent: ethanol/NMP/DMF (as used for LPE)	0D (BNQDs)	—	Low cytotoxicity for bio-imaging; readily integrated into proton-exchange membranes with proton conductivity ↑ and water retention ↑
	Solvothermal amination[84]	BNNS-derived BNQDs; amino ligands (solvent-dependent)	0D (BNQDs)	Surface $-NH_2$	Full-color emission (≈420–610 nm); thermostable, flexible optical films/security labels
	Potassium intercalation (190–200 °C) → brief air de-intercalation → ($EtOH/H_2O$) ultrasonication[78]	Bulk h-BN; K (intercalant)	0D (BNQDs)	—	Blue-green PL; monolayer BNQDs; non-toxic fluorescent labels for confocal bio-imaging
	Ball milling → liquid exfoliation (urea) → hydrothermal cutting → sonication[88]	Bulk h-BN; urea (N source); water/EtOH	0D (BNQDs)	Surface $-NH_2$	BNQDs/rGO (covalent hybrid); supercapacitor: Specific capacitance 90 F g^{-1}@1 A g^{-1}; ↑ carrier conc., sorption, durability
	(H_2O/EtOH/acetone) ultrasonication → hBNNs → solvothermal (DMF, 180 °C, 12 h)[76]	Bulk h-BN; DMF	0D (BNQDs) + 2D (BNNSs)	Oxygenated/DMF-derived surface	Blue PL potential in bio/photoelectric fields
	Microwave irradiation (150 °C, 10 min, 500 W)[77]	h-BN or BN nanosheet suspensions	0D (BNQDs) + 2D (BNNSs)	—	Homogeneous BNQDs; strong microwave absorption
	Polyethylenimine-assisted viscous ball milling[126]	Bulk BN	2D (BNNSs)	—	Scalable monolayer-rich exfoliation
	N-Methylpyrrolidone ball milling → polyvinylidene fluoride film casting[127]	Bulk h-BN	2D (BNNSs)	—	Flexible self-supporting composite films; in-plane TC ≈ 11.88 W m^{-1} K^{-1}, through-plane ≈ 0.41 W m^{-1} K^{-1}
	Hydrothermal exfoliation (Li^+ intercalation; 180 °C, 12 h; strong stirring)[129]	Bulk h-BN; LiCl in IPA	2D (BNNSs)	—	High-yield BNNSs; enhanced TiO_2/MO photodegradation
	Rotating packed bed (shear-driven) in water; (i) polyvinyl alcohol-assisted exfoliation; (ii) NH_4HCO_3 ball-milling pretreatment[125]	h-BN powder	2D (BNNSs)	–OH groups and $-NH_2$ with OH	Water-dispersible functionalized BNNSs
	Aqueous ball milling[134]	BN; tannic acid (plant polyphenol)	2D (BNNSs)	TA grafting	High yield and water solubility; epoxy composites: TC and mechanical strength ↑
	TA-modified BNNSs + BN nanowires into phosphorylated cardanol-based epoxy[147]	BN nanosheets + BN nanowire feedstock + epoxy system	2D (BNNSs) + 1D (BN nanowires)	TA-modified BN	Electronic packaging, improved tensile, smoke suppression, low dielectric loss
Bottom-up	Hydrothermal[83]	Boric acid; melamine	0D (BNQDs)	Oxygenated BNQDs	BNQDs anchored on 3D ZnO; UV dye photodegradation (MB/MO)
	Hydrothermal (200 °C, 12 h; sealed autoclave)[89]	Boric acid; urea EtOH/H_2O; 10% NH_3	0D (BNQDs)	Post-synthesis coat on GCE and	Vitamin C sensing; blue PL; catalytic enhancement on GCE

Table 1 (*Contd.*)

Approach	Method	Precursors/feedstocks	Dimensionality	Functionalized/dopant	Application
				electropolymerize Poly(luminol)	
	Solvothermal (ethanol)[81]	Boric acid; dicyandiamide (cyanoguanidine)	0D (BNQDs)	—	Orthorhombic BNQDs, 2–9 nm; HRTEM lattice spacing ~0.209 nm
	Solvothermal (CCl_4)[82]	Ammonia borane (AB)	0D (BNQDs)	—	QLEDs: PL 386 nm, EL 412 nm
	Vapor-phase laser ablation[97]	Boron fibers; N_2; molten B ball forms, CO_2 laser	1D (BNNTs)	—	Mechanistic insight for synthesis
	Plasma (AB used as volatile feed)[100]	Ammonia borane (AB)	1D (BNNTs)	—	Highly crystalline double-walled BNNTs; less turbostratic BN and negligible h-BN *vs.* h-BN powder feed
	Arc/plasma discharge (carbon-free arc between BN-packed W rod, anode >3427 °C and cooled Cu cathode)[93]	BN-filled tungsten rod	1D (BNNTs)	—	Foundational historical BNNT synthesis route
	Plasma-assisted CVD[104]	Borazine; O_2(essential) over Cu/Cu_2O	1D (BNNTs)	—	Synthesis demonstration; core–shell nanowires
	CVD (Fe_2O_3-catalyzed, ~1050 °C)[99]	Colemanite	1D (BNNTs)	—	Multi-walled BNNTs at comparatively lower T (*vs.* >1200 °C routes)
	CVD (self-catalysis by liquid phase, Li^+ incorporated into W_2B_5 lattice → W–B–Li liquid phase)[101]	W–B–Li (Li^+ in W_2B_5 lattice)	1D (BNNTs)	—	Self-catalyzed high-quality BNNT growth per DFT-MD
	CVD (Al-based catalyst)[102]	Al–B systems	1D (BNNTs)	—	AlB_2 pinpointed as an effective BNNT catalyst; guides low-T/high-yield CVD design
	Staged annealing (lithium borate catalyst, 770–1300 °C; growth at 1300 °C for 0.5–2 h)[98]	Amorphous B; Li_2O (3 : 1 molar) or $Li_2B_4O_7$; Ar/N_2/NH_3	1D (BNNTs)	—	High-quality BNNTs; reduced precursor/NH_3 consumption with high reactivity/flexibility
	Controlled catalytic synthesis of *N*-methyl polyaminoborane → electrospinning → curing/cross-linking intermediate → thermolysis/ammonolysis under NH_3 to convert to h-BN fibers[141]	Monomethylamineborane → *N*-methyl polyaminoborane (THF/$CHCl_3$; NH_3)	1D (h-BN fibers; micro-/nano-fibers)	—	Lightweight, electrically insulating, thermally stable fibrous BN as multifunctional filler
	Ball-milling → high-T NH_3 annealing (1400 °C, 6 h)[128]	$NaBH_4$+NH_4BF_4 (B/N sources)	2D (BNNSs)	—	Large-scale yield ~5–6 g per run of high-purity BNNSs; scalable
	Hydrothermal (pH 8; 180 °C, 12 h)[136]	Boric acid; arginine (1 : 2, H_2O); NaOH	2D (BNNSs)	–OH	Fluorescent uric acid sensor
	NaCl salt-template + spray-dry → NH_3 pyrolysis (900–1200 °C, 3 h, 60 mL min^{-1}) → HNO_3 hydroxylation (70 °C, 18 h)[130]	Boric acid; 2-methylimidazole; NaCl (4 : 3 : 28 in H_2O)	2D (BNNSs)	–OH (post-HNO_3)	Gram-scale BNNSs per run; OH-BNNSs water stablitiy ≥48 h at 1 mg mL^{-1}; cell viability at 100 μg mL^{-1}; *in vivo* tumor inhibition
	CVD (epitaxial growth on single-crystal Ni at high T)[139]	Borazine; Ni(111) foil catalyst/substrate	2D (few-layer) & trilayer hBN (single-crystal, wafer-scale)	—	High-quality dielectric for 2D electronics (MoS_2 FET); also acts as a protective layer during

Table 1 (*Contd.*)

Approach	Method	Precursors/feedstocks	Dimensionality	Functionalized/dopant	Application
					electrochemical hydrogen evolution testing
	LPCVD (monolayer hBN growth on Cu foil with H_2 anneal)[138]	Ammonia borane; Cu foil substrate	Large-area 2D monolayer hBN	—	High-performance 2D electronic/optoelectronic device stacks
	CVD (BN/graphene heterostructure integrated int hollow-core fiber; vertical epitaxy BN grown on graphene)[142]	Optical fiber + graphene layer; (hydroxyl-rich methanol treatment)	2D BN thin film (stacked on graphene)	—	Tunable photonic waveguide; improved all-optical modulation performance
	Single wet impregnation of CF fabric with ammonia–borane/THF → nitridation 2 h at 1000–1500 °C in flowing N_2; h-BN crystallizes ≥1300 °C[143]	Ammonia borane in THF; CF woven fabric substrate; N_2 atmosphere	2D (h-BN film/nanosheet barrier coating) on fibers	—	Oxidation protection for high-T composites (aerospace/hot structures)
Post-synthesis functionalization	Tannic acid deposition on BNNT (aq., pH ≈ 10) → decylamine coupling *via* Michael addition[108]	BNNTs	1D (BNNTs)	TA coating and DA grafting (BNNT-TA-DA)	Dispersion across polar & non-polar solvents; epoxy composite: Tensile +26.8%, strain +52.2%

emphasizing their efficiency as metal-free catalysts in hydrogenation and dehydrogenation reactions.[253]

Owing to its thermal stability, chemical inertness, polar B–N bonds, and 2D morphology, h-BN has garnered significant attention as a catalyst carrier/support. Vacancies and defect-rich h-BN nanosheets provide anchoring sites that improve metal dispersion and enable strong metal–support interactions (SMSI-like), thereby enhancing catalytic performance. Oxidative etching of h-BN sheets generates B_2O_3-like species that can partially encapsulate metal catalysts and modulate adjacent metal sites to facilitate catalysis. Ultra-thin h-BN shells covering metal surfaces serve as 2D nanoreactors, introducing confinement effects and providing novel approaches to modulate metal-catalyzed reactions. An ionothermal route produced h-BN-supported nanocatalysts exhibiting SMSI and robust CO oxidation activity, without relying on reducible metal oxides. These nanocatalysts demonstrated high catalytic efficiency, thermal stability, and sintering resistance under conditions simulating real-world exhaust systems.[253]

DFT simulations evaluated BNNP/Ag nanohybrids, showing that varying surface boron oxide concentrations significantly influence their catalytic activity.[257] The catalytic efficiencies of metal-functionalized BNNTs (f-BNNTs) for removing NO and CO were also investigated under various conditions. Nanoparticle-decorated f-BNNTs were found to potentially reduce the usage of PGM catalysts (Pt, Pd, Rh) while maintaining or exceeding their performance in simultaneous NO and CO removal.[258] Han-Gyu *et al.* employed a V-Cu/BN-Ti catalyst to eliminate residual NH_3 and NO_x; incorporation of h-BN increased surface Cu and V concentrations. This study suggests that h-BN could serve as an effective catalyst for eliminating residual NO_x, aiding compliance with NH_3 emission regulations.[259]

While near-term alternatives to the Haber–Bosch process are unlikely to be commercially viable, renewed interest in alternative non-iron catalysts, particularly ruthenium (Ru)-based systems, is noteworthy. The Ba–Ru/BN catalyst exhibits higher activity than Ru catalysts on graphitic supports, as carbon-supported Ru catalysts are prone to methanation under high H_2 pressures. The thermodynamic stability of BN under harsh test conditions (~100 bar, ~550 °C) contributes to the sustained activity of Ba–Ru/BN catalysts.[260] BN nanomaterials are also stable under harsh electrochemical environments which was utilized by Uosaki *et al.*, who used atomically thin BNNSs as an interfacial layer on a gold electrode to significantly reduce oxygen reduction reaction overpotential.[261] The diverse and promising combinations of h-BN with metal catalysts exemplify the growing potential of heterogeneous catalysis, as highlighted by Dong *et al.*[262]

4 Conclusion summary and future prospects

Boron nitride (BN) nanomaterials have matured into a chemically robust, electrically insulating, and thermally conductive platform spanning zero- to three-dimensional (0D–3D)

architectures. Controlled synthesis through top–down and bottom–up routes, followed by defect/dopant engineering and surface functionalization, now enables deliberate tuning of optical, thermal, electronic, and interfacial properties. This design latitude underpins demonstrated performance in electrochemical, spectrofluorimetric, and chemiluminescent sensing, as well as in adsorption and chromatographic separations; besides various applications, including biomedicine, drug delivery, aerospace radiation shielding, heterogeneous catalysis, and polymer heat spreaders/thermal interface composites. A detailed overview of the BN nanomaterials' synthesis, core properties, functions, and up-to-date applications has been comprehensively reviewed. The review outcomes have been briefly summarized in Fig. 4 and Table 1. The key synthesis parameters, some reported precursors, and typical yields are also summarized in Table 1.

Translational progress will depend on addressing cross-cutting bottlenecks. These include scalable, reproducible synthesis with tight control of defect chemistry and functionalization; standardized metrology for optical stability and composite performance (*e.g.*, quantum yield, filler orientation, percolation, interfacial resistance); reliable dispersion/compatibilization in matrices; and application-specific *in vivo* safety profiles. Addressing these gaps will accelerate the transition from laboratory demonstrations to reliable, manufacturable technologies.

Future progress will benefit from data-driven discoveries, coupled with *operando* characterization. Machine-learning models trained on synthesis–structure–property datasets can guide precursor selection and target defect motifs. Meanwhile, *in situ* spectroscopy and electron microscopy can resolve active sites in metal-free BN catalysis (*e.g.*, B–OH edge radicals) and clarify strong metal–support interactions at metal/BN interfaces.

For optoelectronics and sensing, rational control of BN quantum dots' emissive centers *via* amination, heteroatom doping, and edge engineering is expected to deliver red-shifted, stable, high quantum yield emission with ratiometric readouts compatible with paper/smartphone formats. In thermal management, hierarchical architectures that align BN nanosheets' heat-conduction pathways and minimize interfacial resistance, together with additively manufactured BN lattices, can enhance both in-plane and through-plane conductivity while maintaining dielectric insulation and processability. In energy and environmental technologies, architected BN supports and 2D BN nanoreactors offer durable catalysts for oxidative dehydrogenation and CO_2 conversion. Porous BN and BN nanotubes with tailored pore chemistry offer high capacity, selectivity, and cycling stability for contaminant removal. They also serve as chromatographic stationary-phase modifiers, enhancing resolution and detection. Finally, biomedical translation will require standardized protocols for toxicology, pharmacokinetics, and biodegradation, along with surface chemistry that ensures serum stability, targeting, and predictable clearance.

With coordinated efforts in scalable synthesis, rigorous standards, and application-informed design, BN nanomaterials are positioned to become key enablers across various fields, including sensing, energy, catalysis, aerospace, analysis, and healthcare.

Author contributions

R. K and S. A: investigation, formal analysis, data curation, validation, writing – original draft preparation; S. S: review and editing; A. A: project administration, funding acquisition, writing – review and editing; A. I: conceptualization, data curation, project administration, supervision, and editing writing – review and editing. All authors have read and agreed to the published version of the manuscript.

Conflicts of interest

The authors declare that they have no competing interests.

Abbreviations

BN	Boron nitride
BNNPs	BN nanoparticles
BNNSs	BN nanosheets
BNNTs	BN nanotubes
BNQDs	BN quantum dots
CNT	Carbon nanotube
CVD	Chemical vapor deposition
CL	Chemiluminescence
c-BN	Cubic BN
DA	Decylamine
DL	Detection limit
DW-BNNTs	Double-walled BNNTs
ECL	Electrochemiluminescence
EVA	Ethylene-vinyl acetate
FA	Folic-acid
f-BNNTs	Functionalized BNNTs
GCE	Glassy carbon electrode
HNTs	Halloysite nanotubes
h-BN	hexagonal BN
h-BNNSs	h-BN nanosheets
HPLC	High-performance liquid chromatography
OH-BNNSs	Hydroxylated BNNSs
MEF	Metal-enhanced fluorescence
MDEA	Methyldiethanolamine
NRET	Non-radiative energy transfer
PE	Polyethylene
pHEMA	Polyhydroxyethyl methacrylate
QY	Quantum yield
rGO	Reduced graphene oxide
ssDNA	Single-stranded DNA
SPE	Solid-phase extraction
SMSI	Strong metal–support interactions
TA	Tannic acid
TC	Thermal conductivity
TPU	Thermoplastic polyurethane
0D	Zero-dimensional

Data availability

No primary research results, software or code have been included and no new data were generated or analysed as part of this review.

Supplementary information: history and development milestone for BN nanomaterials. See DOI: https://doi.org/10.1039/d5ra09482h.

Acknowledgements

The authors would like to acknowledge the deanship of scientific research at the University of Nizwa for supporting this research under an internal grant (No. UON/54/IF/2025). During the preparation of this review, some authors utilized AI (Chat GPT and DeepSeek) for grammatical errors correction and improvement of scientific writing. When used, the authors reviewed and edited that content and remain fully responsible for the content published.

References

1 N. Baig, I. Kammakakam and W. Falath, *Mater. Adv.*, 2021, **2**, 1821–1871.
2 H. Sun, L. Wu, N. Gao, J. Ren and X. Qu, *ACS Appl. Mater. Interfaces*, 2013, **5**, 1174–1179.
3 S. Zhu, Q. Meng, L. Wang, J. Zhang, Y. Song, H. Jin, K. Zhang, H. Sun, H. Wang and B. Yang, *Angew. Chem., Int. Ed.*, 2013, **52**, 3953–3957.
4 X. Zhang, H. Wang, H. Wang, Q. Zhang, J. Xie, Y. Tian, J. Wang and Y. Xie, *Adv. Mater.*, 2014, **26**, 4438–4443.
5 Z. Fan, S. Li, F. Yuan and L. Fan, *RSC Adv.*, 2015, **5**, 19773–19789.
6 S. Chung, R. A. Revia and M. Zhang, *Adv. Mater.*, 2021, **33**, 1904362.
7 Q. Zhang, J. Jie, S. Diao, Z. Shao, Q. Zhang, L. Wang, W. Deng, W. Hu, H. Xia, X. Yuan and S.-T. Lee, *ACS Nano*, 2015, **9**, 1561–1570.
8 C. Wang, C. Wu, X. Zhou, T. Han, X. Xin, J. Wu, J. Zhang and S. Guo, *Sci. Rep.*, 2013, **3**, 2852.
9 Z. Gu, S. Zhu, L. Yan, F. Zhao and Y. Zhao, *Adv. Mater.*, 2019, **31**, 1800662.
10 A. Saha, K. V. Chellappan, K. S. Narayan, J. Ghatak, R. Datta and R. Viswanatha, *J. Phys. Chem. Lett.*, 2013, **4**, 3544–3549.
11 Q. Zhang, C. Nie, C. Chang, C. Guo, X. Jin, Y. Qin, F. Li and Q. Li, *Opt. Mater. Express*, 2017, **7**, 3875–3884.
12 H. Li, X. He, Z. Kang, H. Huang, Y. Liu, J. Liu, S. Lian, C. H. A. Tsang, X. Yang and S.-T. Lee, *Angew. Chem., Int. Ed.*, 2010, **49**, 4430–4434.
13 H. Labiadh, T. B. Chaabane, L. Balan, N. Becheik, S. Corbel, G. Medjahdi and R. Schneider, *Appl. Catal. B Environ.*, 2014, **144**, 29–35.
14 B. I. Salman, H. A. Batakoushy, R. E. Saraya, A. I. Hassan, A. Al-Harrasi and A. E. Ibrahim, *Talanta*, 2025, **292**, 128014.
15 H. A. Batakoushy, A. K. A. Bass, H. Gomaa, S. El Deeb and A. E. Ibrahim, *Biosensors*, 2025, **15**, 263.
16 S. Ge, F. Lan, F. Yu and J. Yu, *New J. Chem.*, 2015, **39**, 2380–2395.
17 A. Kausar, I. Rafique and B. Muhammad, *Polym.-Plast. Technol. Eng.*, 2017, **56**, 1438–1456.
18 X. Blase, A. Rubio, S. G. Louie and M. L. Cohen, *Europhys. Lett.*, 1994, **28**, 335.
19 J. S. Lauret, R. Arenal, F. Ducastelle, A. Loiseau, M. Cau, B. Attal-Tretout, E. Rosencher and L. Goux-Capes, *Phys. Rev. Lett.*, 2005, **94**, 037405.
20 M. I. Petrescu and M. Balint, *Sci. Bull. B Chem. Mater. Sci. UPB*, 2007, **69**, 35–42.
21 C. Zhi, Y. Bando, T. Terao, C. Tang, H. Kuwahara and D. Golberg, *Adv. Funct. Mater.*, 2009, **19**, 1857–1862.
22 W. H. Balmain, *Lond. Edinb. Dubl. Phil. Mag.J. Sci.*, 1842, **21**, 270–277.
23 R. S. Ruoff and D. C. Lorents, *Carbon*, 1995, **33**, 925–930.
24 Y. Chen, J. Zou, S. J. Campbell and G. Le Caer, *Appl. Phys. Lett.*, 2004, **84**, 2430–2432.
25 C. W. Chang, A. M. Fennimore, A. Afanasiev, D. Okawa, T. Ikuno, H. Garcia, D. Li, A. Majumdar and A. Zettl, *Phys. Rev. Lett.*, 2006, **97**, 085901.
26 D. A. Stewart, I. Savić and N. Mingo, *Nano Lett.*, 2009, **9**, 81–84.
27 W. Jang, S. Lee, N. R. Kim, H. Koo, J. Yu and C.-M. Yang, *Composites, Part B*, 2023, **248**, 110355.
28 C. Cazorla and T. Gould, *Sci. Adv.*, 2019, **5**, eaau5832.
29 D. Gonzalez Ortiz, C. Pochat-Bohatier, J. Cambedouzou, M. Bechelany and P. Miele, *Nanomaterials*, 2018, **8**, 716.
30 M. Emanet, Ö. Sen, I. Ç. Taşkin and M. Çulha, *Front. Bioeng. Biotechnol.*, 2019, 7–2019.
31 Y. F. Hassan, E. Alzahrani, M. A. Abdel-Lateef, B. I. Salman and A. E. Ibrahim, *J. Fluoresc.*, 2025, **35**, 4291–4300.
32 J. Uddin, R. Dubey, V. S. Balasubramaniam, J. Kabel, V. Khare, Z. Salimi, S. Sharma, D. Zhang and Y. K. Yap, *Micromachines*, 2024, **15**, 349.
33 M. Topsakal, E. Aktürk and S. Ciraci, *Phys. Rev. B:Condens. Matter Mater. Phys.*, 2009, **79**, 115442.
34 S. Roy, X. Zhang, A. B. Puthirath, A. Meiyazhagan, S. Bhattacharyya, M. M. Rahman, G. Babu, S. Susarla, S. K. Saju, M. K. Tran, L. M. Sassi, M. A. S. R. Saadi, J. Lai, O. Sahin, S. M. Sajadi, B. Dharmarajan, D. Salpekar, N. Chakingal, A. Baburaj, X. Shuai, A. Adumbumkulath, K. A. Miller, J. M. Gayle, A. Ajnsztajn, T. Prasankumar, V. V. J. Harikrishnan, V. Ojha, H. Kannan, A. Z. Khater, Z. Zhu, S. A. Iyengar, P. A. d. S. Autreto, E. F. Oliveira, G. Gao, A. G. Birdwell, M. R. Neupane, T. G. Ivanov, J. Taha-Tijerina, R. M. Yadav, S. Arepalli, R. Vajtai and P. M. Ajayan, *Adv. Mater.*, 2021, **33**, 2101589.
35 D. V. Shtansky, A. T. Matveev, E. S. Permyakova, D. V. Leybo, A. S. Konopatsky and P. B. Sorokin, *Nanomaterials*, 2022, **12**, 2810.
36 M. Li, G. Huang, X. Chen, J. Yin, P. Zhang, Y. Yao, J. Shen, Y. Wu and J. Huang, *Nano Today*, 2022, **44**, 101486.
37 O. Hod, *J. Chem. Theory Comput.*, 2012, **8**, 1360–1369.
38 H. J. Park, J. Cha, M. Choi, J. H. Kim, R. Y. Tay, E. H. T. Teo, N. Park, S. Hong and Z. Lee, *Sci. Adv.*, 2020, **6**, eaay4958.

39 J. Cao, T. L. Meng, X. Zhang, C. K. I. Tan, A. Suwardi and H. Liu, *Mater. Today Electron.*, 2022, **2**, 100005.
40 A. Hayat, M. Sohail, M. S. Hamdy, T. A. Taha, H. S. AlSalem, A. M. Alenad, M. A. Amin, R. Shah, A. Palamanit, J. Khan, W. I. Nawawi and S. K. B. Mane, *Surf. Interfaces*, 2022, **29**, 101725.
41 Y. Lin, T. V. Williams, T.-B. Xu, W. Cao, H. E. Elsayed-Ali and J. W. Connell, *J. Phys. Chem. C*, 2011, **115**, 2679–2685.
42 B. Yu, W. Xing, W. Guo, S. Qiu, X. Wang, S. Lo and Y. Hu, *J. Mater. Chem. A*, 2016, **4**, 7330–7340.
43 Z. Zheng, M. Cox and B. Li, *J. Mater. Sci.*, 2018, **53**, 66–99.
44 J. Ren, L. Stagi and P. Innocenzi, *J. Mater. Sci.*, 2021, **56**, 4053–4079.
45 A. Merlo, V. R. S. S. Mokkapati, S. Pandit and I. Mijakovic, *Biomater. Sci.*, 2018, **6**, 2298–2311.
46 H. N. Gurbuz, K. Yilmaz, H. H. Ipekci, A. Uzunoglu and E. M. Cagil, *Mater. Sci. Eng. B*, 2024, **299**, 116909.
47 J. Wang, F. Ma, W. Liang and M. Sun, *Mater. Today Phys.*, 2017, **2**, 6–34.
48 V. Sharma, H. L. Kagdada, P. K. Jha, P. Śpiewak and K. J. Kurzydłowski, *Renew. Sustain. Energy Rev.*, 2020, **120**, 109622.
49 D. Pan, F. Su, H. Liu, Y. Ma, R. Das, Q. Hu, C. Liu and Z. Guo, *Chem. Rec.*, 2020, **20**, 1314–1337.
50 D. Golberg, Y. Bando, Y. Huang, T. Terao, M. Mitome, C. Tang and C. Zhi, *ACS Nano*, 2010, **4**, 2979–2993.
51 T.-H. Le, Y. Oh, H. Kim and H. Yoon, *Chem.–Eur. J.*, 2020, **26**, 6360–6401.
52 C. Gautam and S. Chelliah, *RSC Adv.*, 2021, **11**, 31284–31327.
53 I. G. Juma, G. Kim, D. Jariwala and S. K. Behura, *iScience*, 2021, **24**, 103374.
54 X. Shen, Q. Zheng and J.-K. Kim, *Prog. Mater. Sci.*, 2021, **115**, 100708.
55 M. J. Meziani, K. Sheriff, P. Parajuli, P. Priego, S. Bhattacharya, A. M. Rao, J. L. Quimby, R. Qiao, P. Wang, S.-J. Hwu, Z. Wang and Y.-P. Sun, *ChemPhysChem*, 2022, **23**, e202100645.
56 P. M. Revabhai, R. K. Singhal, H. Basu and S. K. Kailasa, *J. Nanostruct. Chem.*, 2022, **13**, 1–41.
57 Y. Yang, Y. Peng, M. F. Saleem, Z. Chen and W. Sun, *Materials*, 2022, **15**, 4396.
58 S. Bernard and P. Miele, *Materials*, 2014, **7**, 7436–7459.
59 J. Pu, K. Zhang, Z. Wang, C. Li, K. Zhu, Y. Yao and G. Hong, *Adv. Funct. Mater.*, 2021, **31**, 2106315.
60 M. Shimomura and T. Sawadaishi, *Curr. Opin. Colloid Interface Sci.*, 2001, **6**, 11–16.
61 S. Choudhury, S. Paul, S. Goswami and K. Deb, in *Advances in Nanotechnology-Based Drug Delivery Systems*, ed. A. Das Talukdar, S. Dey Sarker and J. K. Patra, Elsevier, 2022, pp. 21–44, DOI: 10.1016/B978-0-323-88450-1.00005-3.
62 J. Wang and N. Li, *J. Mater. Chem. B*, 2017, **5**, 8430–8445.
63 J. Drbohlavova, V. Adam, R. Kizek and J. Hubalek, *Int. J. Mol. Sci.*, 2009, **10**, 656–673.
64 X. Zhang, L. An, C. Bai, L. Chen and Y. Yu, *Mater. Today Chem.*, 2021, **20**, 100425.
65 A. Kalkal, S. Kadian, R. Pradhan, G. Manik and G. Packirisamy, *Mater. Adv.*, 2021, **2**, 5513–5541.
66 S.-Y. Liao, J. Chen, S.-F. Cui, J.-Q. Shang, Y.-Z. Li, W.-X. Cheng, Y.-D. Liu, T.-T. Cui, X.-G. Shu and Y.-G. Min, *J. Power Sources*, 2023, **553**, 232265.
67 B. I. Salman, A. I. Hassan, A. Al-Harrasi, A. E. Ibrahim and R. E. Saraya, *Anal. Chim. Acta*, 2024, **1327**, 343175.
68 T. Adschiri, Y.-W. Lee, M. Goto and S. Takami, *Green Chem.*, 2011, **13**, 1380–1390.
69 N. I. Kovtyukhova, Y. Wang, R. Lv, M. Terrones, V. H. Crespi and T. E. Mallouk, *J. Am. Chem. Soc.*, 2013, **135**, 8372–8381.
70 H. Li, R. Y. Tay, S. H. Tsang, X. Zhen and E. H. T. Teo, *Small*, 2015, **11**, 6491–6499.
71 P. Thangasamy, M. Santhanam and M. Sathish, *ACS Appl. Mater. Interfaces*, 2016, **8**, 18647–18651.
72 F. I. Alzakia and S. C. Tan, *Adv. Sci.*, 2021, **8**, 2003864.
73 Z. Lei, S. Xu, J. Wan and P. Wu, *Nanoscale*, 2015, **7**, 18902–18907.
74 R. Kumar, R. K. Singh, S. K. Yadav, R. Savu and S. A. Moshkalev, *J. Alloys Compd.*, 2016, **683**, 38–45.
75 V. Štengl, J. Henych and M. Kormunda, *Sci. Adv. Mater.*, 2014, **6**, 1106–1116.
76 L. Chen, X. Zhang, Z. Zhao, F. Wang, Y. Huang, C. Bai, L. An and Y. Yu, *Colloids Surf. A Physicochem. Eng. Asp.*, 2021, **614**, 126181.
77 L. Fan, Y. Zhou, M. He, Y. Tong, X. Zhong, J. Fang and X. Bu, *J. Mater. Sci.*, 2017, **52**, 13522–13532.
78 L. Lin, Y. Xu, S. Zhang, I. M. Ross, A. C. M. Ong and D. A. Allwood, *Small*, 2014, **10**, 60–65.
79 D. L. Duong, S. J. Yun and Y. H. Lee, *ACS Nano*, 2017, **11**, 11803–11830.
80 J. Yang, S. Zhu, D. Zhao, X. Rong, X. Zhang, N. Zhao and C. He, *Sci. China Mater.*, 2025, **68**, 3114–3142.
81 P. Chen, S. Yang, F. Liu, Y. Jiang, Y. Wang, Y. Huang, J. Hu and L. Chen, *Adv. Photonics Res.*, 2023, **4**, 2200344.
82 P. Chen, S. Yang, F. Liu, C. Han, J. Hu, Y. Jiang and L. Chen, *Appl. Mater. Today*, 2023, **31**, 101744.
83 D. Liu, J. Song, J. S. Chung, S. H. Hur and W. M. Choi, *Molecules*, 2022, **27**, 6833.
84 Y. Ding, P. He, S. Li, B. Chang, S. Zhang, Z. Wang, J. Chen, J. Yu, S. Wu, H. Zeng and L. Tao, *ACS Nano*, 2021, **15**, 14610–14617.
85 J. Y. Jung, Y.-S. Shim, C. S. Son, Y.-K. Kim and D. Hwang, *ACS Appl. Nano Mater.*, 2021, **4**, 3529–3536.
86 S. Mishra and B. K. Jena, *Energy Fuels*, 2025, **39**, 4119–4150.
87 S. Sasikumar and A. Rajaram, *J. Photochem. Photobiol., A*, 2026, **470**, 116670.
88 J. W. Lee, T. Kshetri, K. R. Park, N. H. Kim, O.-K. Park and J. H. Lee, *Composites, Part B*, 2021, **222**, 109089.
89 R. Jerome and A. K. Sundramoorthy, *J. Electrochem. Soc.*, 2019, **166**, B3017.
90 B. Sert, S. Gonca, Y. Ozay, E. Harputlu, S. Ozdemir, K. Ocakoglu and N. Dizge, *Colloids Surf., B*, 2021, **205**, 111867.
91 J. H. Kim, T. V. Pham, J. H. Hwang, C. S. Kim and M. J. Kim, *Nano Convergence*, 2018, **5**, 17.

92 S. Silva-Santos, A. Impellizzeri, A. Aguiar, C. Journet, C. Dalverny, B. Toury, J. de Sousa, C. Ewels and A. San-Miguel, *J. Phys. Chem. C*, 2021, **125**, 11440–11453.
93 N. G. Chopra, R. J. Luyken, K. Cherrey, V. H. Crespi, M. L. Cohen, S. G. Louie and A. Zettl, *Science*, 1995, **269**, 966–967.
94 A. Loiseau, F. Willaime, N. Demoncy, G. Hug and H. Pascard, *Phys. Rev. Lett.*, 1996, **76**, 4737–4740.
95 Y. Saito, M. Maida and T. Matsumoto, *Jpn. J. Appl. Phys.*, 1999, **38**, 159.
96 J. Cumings and A. Zettl, *Chem. Phys. Lett.*, 2000, **316**, 211–216.
97 J. H. Kim, H. Cho, T. V. Pham, J. H. Hwang, S. Ahn, S. G. Jang, H. Lee, C. Park, C. S. Kim and M. J. Kim, *Sci. Rep.*, 2019, **9**, 15674.
98 K. Zhang, P. Xue, J. Wu, L. Wu, N. Wang, T. Xu, K. Zhu, J. Pu, Q. Li, Y. Deng, Y. Yao and J. Zhang, *Chem. Mater.*, 2023, **35**, 4857–4864.
99 D. Köken, P. Sungur, H. Cebeci and F. Ç. Cebeci, *ACS Appl. Nano Mater.*, 2022, **5**, 2137–2146.
100 D. Bae, U. Jung, H. Lee, H. Yoo, S. Y. Moon, K.-H. Lee and M. J. Kim, *ACS Omega*, 2023, **8**, 21514–21521.
101 N. Wang, L. Ding, T. Li, K. Zhang, L. Wu, Z. Zhou, Q. He, X. He, X. Wang, Y. Hu, F. Ding, J. Zhang and Y. Yao, *Small*, 2023, **19**, 2206933.
102 Q. He, L. Ding, L. Wu, Z. Zhou, Y. Wang, T. Xu, N. Wang, K. Zhang, X. Wang, F. Ding, J. Zhang and Y. Yao, *Small Structures*, 2023, **4**, 2200282.
103 A. Alrebh, D. Ruth, M. Plunkett, L. Gaburici, M. Couillard, T. Lacelle, C. T. Kingston and K. S. Kim, *Chem. Eng. J.*, 2023, **472**, 144891.
104 T. Shiratori, I. Yamane, S. Nodo, R. Ota, T. Yanase, T. Nagahama, Y. Yamamoto and T. Shimada, *Nanomaterials*, 2021, **11**, 651.
105 C. Sun, H. Yu, L. Xu, Q. Ma and Y. Qian, *J. Nanomater.*, 2010, **2010**, 163561.
106 C. Aguiar, M. Camps, N. Dattani and I. Camps, *Appl. Surf. Sci.*, 2023, **611**, 155358.
107 J. Sneha, R. M. Hariharan, R. Akash, A. S. Balaji, D. J. Thiruvadigal, U. Adharsh, V. Abinaya and K. J. Sivasankar, *Surf. Interfaces*, 2023, **42**, 103337.
108 Z. Hanif, K.-I. Choi, J.-H. Jung, A. G. M. Pornea, E. Park, J. Cha, H.-R. Kim, J.-H. Choi and J. Kim, *Ind. Eng. Chem. Res.*, 2023, **62**, 2662–2670.
109 G. Ciofani, V. Raffa, A. Menciassi and A. Cuschieri, *Nano Today*, 2009, **4**, 8–10.
110 X. Zeng, J. Sun, Y. Yao, R. Sun, J.-B. Xu and C.-P. Wong, *ACS Nano*, 2017, **11**, 5167–5178.
111 D. Gia Ninh, N. Trong Long, T. Van Vang, N. Hoang Ha, C. Thanh Nguyen and D. Viet Dao, *Compos. Struct.*, 2023, **303**, 116239.
112 X. Guo, N. Li, X. Yang, R. Qi, C. Wu, R. Shi, Y. Li, Y. Huang, F. J. García de Abajo, E.-G. Wang, P. Gao and Q. Dai, *Nat. Nanotechnol.*, 2023, **18**, 529–534.
113 D. Yadav, J.-H. Jung, Y. Lee, T. Y.-S. Kim, E. Park, K.-I. Choi, J. Cha, W.-J. Song, J.-H. Choi, S. Doo and J. Kim, *ACS Mater. Lett.*, 2023, **5**, 2648–2655.
114 L. Li, N. Shi, X. Jiang, W. Chen, C. Ban and J. Hao, *ACS Appl. Mater. Interfaces*, 2023, **15**, 31812–31823.
115 W. Luo, Y. Wang, E. Hitz, Y. Lin, B. Yang and L. Hu, *Adv. Funct. Mater.*, 2017, **27**, 1701450.
116 Y. Zhan, J. Yan, M. Wu, L. Guo, Z. Lin, B. Qiu, G. Chen and K.-y. Wong, *Talanta*, 2017, **174**, 365–371.
117 M. Wu, Y. Zhou, H. Zhang and W. Liao, *Adv. Mater. Interfaces*, 2022, **9**, 2200610.
118 P. Ares, T. Cea, M. Holwill, Y. B. Wang, R. Roldán, F. Guinea, D. V. Andreeva, L. Fumagalli, K. S. Novoselov and C. R. Woods, *Adv. Mater.*, 2020, **32**, 1905504.
119 Q. Cai, S. Mateti, H. Jiang, L. H. Li, S. Huang and Y. Chen, *Mater. Today Phys.*, 2022, **22**, 100575.
120 E. Wagemann, Y. Wang, S. Das and S. K. Mitra, *Phys. Chem. Chem. Phys.*, 2020, **22**, 7710–7718.
121 D. Steiner, F. Mittendorfer and E. Bertel, *ACS Nano*, 2019, **13**, 7083–7090.
122 X. Tian, N. Wu, B. Zhang, Y. Wang, Z. Geng and Y. Li, *Chem. Eng. J.*, 2021, **408**, 127360.
123 Z.-G. Wang, X. Wei, M.-H. Bai, J. Lei, L. Xu, H.-D. Huang, J. Du, K. Dai, J.-Z. Xu and Z.-M. Li, *ACS Sustain. Chem. Eng.*, 2021, **9**, 11155–11162.
124 H. Chand, A. Kumar, P. Bhumla, B. R. Naik, V. Balakrishnan, S. Bhattacharya and V. Krishnan, *Adv. Mater. Interfaces*, 2022, **9**, 2200508.
125 Q. Shan, X. Shi, X. Wang and W. Wu, *Chem. Eng. Process.*, 2021, **169**, 108602.
126 Z. Wang, X. Yan, Q. Hou, Y. Liu, X. Zeng, Y. Kang, W. Zhao, X. Li, S. Yuan, R. Qiu, M. H. Uddin, R. Wang, Y. Xia, M. Jian, Y. Kang, L. Gao, S. Liang, J. Z. Liu, H. Wang and X. Zhang, *Nat. Commun.*, 2023, **14**, 236.
127 C. Teng, L. Su, J. Chen and J. Wang, *Compos. Appl. Sci. Manuf.*, 2019, **124**, 105498.
128 Y. Xue, X. Jin, Y. Fan, R. Tian, X. Xu, J. Li, J. Lin, J. Zhang, L. Hu and C. Tang, *Polym. Compos.*, 2014, **35**, 1707–1715.
129 N. Wang, G. Yang, H. Wang, C. Yan, R. Sun and C.-P. Wong, *Mater. Today*, 2019, **27**, 33–42.
130 Y. Cheng, Y. Han, W. Zhang, L. Zeng, Y. Long, S. Wang and Q. Weng, *Chem. Eng. J.*, 2022, **437**, 135304.
131 M. K. Gupta, J. Bijwe and M. Padhan, *Lubr. Sci.*, 2018, **30**, 441–456.
132 X. Fan, C. Gan, P. Feng, X. Ma, Z. Yue, H. Li, W. Li and M. Zhu, *Chem. Eng. J.*, 2022, **431**, 133482.
133 J. Sun, X. Xiao, Y. Zhang, W. Cao, N. Wang and L. Gu, *Ind. Eng. Chem. Res.*, 2022, **61**, 8091–8100.
134 N. Wu, W. Yang, S. Che, L. Sun, H. Li, G. Ma, Y. Sun, H. Liu, X. Wang and Y. Li, *Compos. Appl. Sci. Manuf.*, 2023, **164**, 107266.
135 M. Liao, P. Nicolini, L. Du, J. Yuan, S. Wang, H. Yu, J. Tang, P. Cheng, K. Watanabe, T. Taniguchi, L. Gu, V. E. P. Claerbout, A. Silva, D. Kramer, T. Polcar, R. Yang, D. Shi and G. Zhang, *Nat. Mater.*, 2022, **21**, 47–53.
136 P. M. Revabhai, T. J. Park and S. K. Kailasa, *Inorg. Chem. Commun.*, 2023, **148**, 110346.
137 S. Daneshnia, M. Adeli, A. Yari, A. Shams, I. S. Donskyi and W. E. S. Unger, *Mater. Res. Express*, 2019, **6**, 095076.

138 Y. Wen, X. Shang, J. Dong, K. Xu, J. He and C. Jiang, *Nanotechnology*, 2015, **26**, 275601.
139 K. Y. Ma, L. Zhang, S. Jin, Y. Wang, S. I. Yoon, H. Hwang, J. Oh, D. S. Jeong, M. Wang, S. Chatterjee, G. Kim, A. R. Jang, J. Yang, S. Ryu, H. Y. Jeong, R. S. Ruoff, M. Chhowalla, F. Ding and H. S. Shin, *Nature*, 2022, **606**, 88–93.
140 S. Cheng, H. Zhang, X. Chen, Y. Wang, F. Cheng, P. Sun, Y. Li, Z. Yang, J. Zhang, J. Sun, J. Shao and B. Lu, *Adv. Fiber Mater.*, 2025, **7**, 1302–1316.
141 P.-Y. Lee, B. M. Maciejewska, M. J. Cross, C. M. van Beek, C. N. Brodie, A. S. Bhaskaran, G. T. Tebbutt, R. M. Schofield, S. J. Page, E. Darnbrough, M. Swart, A. S. Weller and N. Grobert, *Adv. Compos. Hybrid Mater.*, 2025, **8**, 392.
142 Y. Cheng, X. Cheng, J. Xie, G. Cui, S. Cheng, X. Li, J. Gan, H. Dong, Y. Yang, W. Yu, K. Chen, H. Hong, X. Zhou, M. Pang, X. Jiang, Z. Sun, K. Liu and Z. Liu, *J. Am. Chem. Soc.*, 2025, **147**, 33735–33742.
143 C. Yıldırım Elçin, M. N. Arık, K. Örs, U. Nakaş, Z. B. Yakışık Özgüle, Ö. Acar, S. Aslanlar, Ö. Altay, E. Çelik and K. Şahin, *J. Compos. Sci.*, 2025, **9**, 564.
144 J. Chen, Y. Cheng, P. Scotland, J. Shin, L. Castelli, J. T. Li, W. Chen, K. M. Wyss, Q. Liu, O. E. Onah, G. Wehmeyer, Y. Zhao and J. M. Tour, *ACS Nano*, 2025, **19**, 24904–24911.
145 K. Orikasa, L. Benedetti, S.-H. Chu, T. Dolmetsch, A. Jimenez, D. John, T. Smith, T. Thomas, B. Boesl, C. Park and A. Agarwal, *Compos. Sci. Technol.*, 2025, **261**, 110995.
146 M. G. Rasul, A. Kiziltas, B. Arfaei and R. Shahbazian-Yassar, *npj 2D Mater. Appl.*, 2021, **5**, 56.
147 G.-L. Wu, Y. Li, Z.-T. Xiao, H.-J. Shi, Y. Hu, Z. Gui and X. Wang, *Compos. Appl. Sci. Manuf.*, 2026, **201**, 109392.
148 J. Li, J. Lin, X. Xu, X. Zhang, Y. Xue, J. Mi, Z. Mo, Y. Fan, L. Hu, X. Yang, J. Zhang, F. Meng, S. Yuan and C. Tang, *Nanotechnology*, 2013, **24**, 155603.
149 H. Cho, J. H. Kim, J. H. Hwang, C. S. Kim, S. G. Jang, C. Park, H. Lee and M. J. Kim, *Sci. Rep.*, 2020, **10**, 7416.
150 B. Zhong, Y. Cheng, M. Wang, Y. Bai, X. Huang, Y. Yu, H. Wang and G. Wen, *Compos. Appl. Sci. Manuf.*, 2018, **112**, 515–524.
151 H. Zeng, C. Zhi, Z. Zhang, X. Wei, X. Wang, W. Guo, Y. Bando and D. Golberg, *Nano Lett.*, 2010, **10**, 5049–5055.
152 K. Watanabe, T. Taniguchi, T. Niiyama, K. Miya and M. Taniguchi, *Nat. Photonics*, 2009, **3**, 591–594.
153 D. Qin, Y. Zhou, W. Wang, C. Zhang, G. Zeng, D. Huang, L. Wang, H. Wang, Y. Yang, L. Lei, S. Chen and D. He, *J. Mater. Chem. A*, 2020, **8**, 19156–19195.
154 Y. Yang, X. Liu, Z. Zhu, Y. Zhong, Y. Bando, D. Golberg, J. Yao and X. Wang, *Joule*, 2018, **2**, 1075–1094.
155 T. T. Tran, K. Bray, M. J. Ford, M. Toth and I. Aharonovich, *Nat. Nanotechnol.*, 2016, **11**, 37–41.
156 F. Hayee, L. Yu, J. L. Zhang, C. J. Ciccarino, M. Nguyen, A. F. Marshall, I. Aharonovich, J. Vučković, P. Narang, T. F. Heinz and J. A. Dionne, *Nat. Mater.*, 2020, **19**, 534–539.
157 D. Golberg, Y. Bando, K. Kurashima and T. Sato, *Scr. Mater.*, 2001, **44**, 1561–1565.
158 M. Azeem, R. Jan, S. Farrukh and A. Hussain, *Results Phys.*, 2019, **12**, 1535–1541.
159 C. R. Dean, A. F. Young, I. Meric, C. Lee, L. Wang, S. Sorgenfrei, K. Watanabe, T. Taniguchi, P. Kim, K. L. Shepard and J. Hone, *Nat. Nanotechnol.*, 2010, **5**, 722–726.
160 Y. Xiao, X. H. Yan, J. X. Cao, J. W. Ding, Y. L. Mao and J. Xiang, *Phys. Rev. B:Condens. Matter Mater. Phys.*, 2004, **69**, 205415.
161 O. Ergen, *AIP Adv.*, 2020, **10**, 045040.
162 D. Kim, X. Liu, B. Yu, S. Mateti, L. A. O'Dell, Q. Rong and Y. Chen, *Adv. Funct. Mater.*, 2020, **30**, 1910813.
163 D. Kim, Rational design of all-solid-state lithium metal batteries, PhD thesis, Deakin University, 2023.
164 J. Ji, S. Yan, Z. Zhou, Y. Gu, C. Liu, S. Yang, D. Wang, Y. Xue and C. Tang, *J. Mater. Sci. Technol.*, 2025, **218**, 170–179.
165 S. M. Z. Mehdi, M. F. Maqsood, A. Dahshan, S. Ahmad, M. U. Rehman, N. Lee, M. A. Rehman and M. F. Khan, *Rev. Adv. Mater. Sci.*, 2024, **63**, 20240075.
166 A. M. E. Hassan, T. A. Ali, G. G. Mohamed, F. M. Ahmed, A. E. Ibrahim, S. El Deeb, B. I. Salman and H. A. Batakoushy, *Microchem. J.*, 2023, **192**, 108905.
167 Q. Weng, X. Wang, X. Wang, Y. Bando and D. Golberg, *Chem. Soc. Rev.*, 2016, **45**, 3989–4012.
168 S. Angizi, M. Khalaj, S. A. A. Alem, A. Pakdel, M. Willander, A. Hatamie and A. Simchi, *J. Electrochem. Soc.*, 2020, **167**, 126513.
169 H. Sohrabi, O. Arbabzadeh, M. Falaki, V. Vatanpour, M. R. Majidi, N. Kudaibergenov, S. W. Joo and A. Khataee, *Surf. Interfaces*, 2023, **41**, 103152.
170 A. A. Ensafi, M. Sohrabi, M. Jafari-Asl and B. Rezaei, *Appl. Surf. Sci.*, 2015, **356**, 301–307.
171 Y. Liu, M. Wang, Y. Nie, Q. Zhang and Q. Ma, *Anal. Chem.*, 2019, **91**, 6250–6258.
172 C. Wang, M. Li, P. Wang and D. Liu, *Microchim. Acta*, 2020, **187**, 409.
173 M. A. Kamyabi and M. Moharramnezhad, *Microchem. J.*, 2021, **168**, 106518.
174 M. A. Kamyabi and M. Moharramnezhad, *Microchim. Acta*, 2021, **188**, 93.
175 D. Qin, X. Jiang, G. Mo, J. Feng and B. Deng, *Electrochim. Acta*, 2020, **335**, 135621.
176 G. Sridharan, C. J. T. Godwin, R. Atchudan, S. Arya, M. Govindasamy, S. M. Osman and A. K. Sundramoorthy, *J. Taiwan Inst. Chem. Eng.*, 2024, **163**, 105320.
177 R. Jerome and A. K. Sundramoorthy, *Anal. Chim. Acta*, 2020, **1132**, 110–120.
178 T. Kokulnathan, T.-J. Wang, E. A. Kumar, N. Duraisamy and L. An-Ting, *Sens. Actuators, B*, 2021, **349**, 130787.
179 Y.-J. Lee, S.-C. Lee, S. C. Jee, J.-S. Sung and A. A. Kadam, *Colloids Surf., B*, 2019, **173**, 18–26.
180 T. Kokulnathan, T.-J. Wang, M. Thangapandian and S. O. Alaswad, *Appl. Clay Sci.*, 2020, **187**, 105483.
181 T. Kokulnathan, R. Vishnuraj, T.-J. Wang, E. A. Kumar and B. Pullithadathil, *Ecotoxicol. Environ. Saf.*, 2021, **207**, 111276.
182 M. L. Yola and N. Atar, *J. Electrochem. Soc.*, 2018, **165**, H897.

183 N. Atar and M. L. Yola, *J. Electrochem. Soc.*, 2018, **165**, H255.
184 W. Gan, C. Tserkezis, Q. Cai, A. Falin, S. Mateti, M. Nguyen, I. Aharonovich, K. Watanabe, T. Taniguchi, F. Huang, L. Song, L. Kong, Y. Chen and L. H. Li, *ACS Nano*, 2019, **13**, 12184–12191.
185 X. Yang, D. H. Shin, Z. Yu, K. Watanabe, T. Taniguchi, V. Babenko, S. Hofmann and S. Caneva, *ChemNanoMat*, 2024, **10**, e202300592.
186 X. Li, S. Chen, Q. Liu, Y. Luo and X. Sun, *Chem. Commun.*, 2021, **57**, 8039–8042.
187 F. Nemati and M. Hosseini, *Microchem. J.*, 2021, **168**, 106346.
188 D. Dabur, M. Arshad, S. Piracha and H.-F. Wu, *Microchem. J.*, 2024, **200**, 110319.
189 L. Wang, Q. Zhang, P. Su, L. Yu, Y. Bu, C. Yuan and S. Wang, *Anal. Chim. Acta*, 2022, **1236**, 340585.
190 D. Peng, L. Zhang, F.-F. Li, W.-R. Cui, R.-P. Liang and J.-D. Qiu, *ACS Appl. Mater. Interfaces*, 2018, **10**, 7315–7323.
191 R. Shokri, M. Amjadi and J. L. Manzoori, *Microchem. J.*, 2022, **181**, 107759.
192 I. Ihsanullah, *Chemosphere*, 2021, **263**, 127970.
193 H. Zhang, Y. Liu, K. Sun, S. Li, J. Zhou, S. Liu, H. Wei, B. Liu, L. Xie, B. Li and J. Jiang, *EnergyChem*, 2023, **5**, 100108.
194 S. A. Shevlin and Z. X. Guo, *Appl. Phys. Lett.*, 2006, **89**, 153104.
195 R. J. Baierle, P. Piquini, T. M. Schmidt and A. Fazzio, *J. Phys. Chem. B*, 2006, **110**, 21184–21188.
196 A. Ranjbar Aghjehkohal, A. Taghizadeh Tabrizi and M. Yildiz, *J. Alloys Compd.*, 2023, **962**, 171159.
197 A. H. Aref and S. Shahhosseini, *Gas Sci. Eng.*, 2023, **111**, 204917.
198 H. Liu, J. Yin, J. Zhang, H. Ran, N. Lv, W. Jiang, H. Li, W. Zhu and H. Li, *Nanomaterials*, 2022, **12**, 2046.
199 F. Liu, Q. Zhou, Y. Li and J. Pang, *Nanomaterials*, 2022, **12**, 318.
200 Y. Pang, X. Zang, M. Wang, Q. Chang, S. Zhang, C. Wang and Z. Wang, *Microchim. Acta*, 2018, **185**, 561.
201 X. Di, N. Li, M.-J. Li, X. Wang, H.-L. Jiang, L.-X. Zhao, X. Chen, J.-M. Lin and R.-S. Zhao, *J. Chromatogr. A*, 2022, **1682**, 463519.
202 M. Fu, H. Xing, X. Chen, F. Chen, C.-M. L. Wu, R. Zhao and C. Cheng, *J. Chromatogr. A*, 2014, **1369**, 181–185.
203 Y. C. Guillaume and C. André, *Talanta*, 2017, **164**, 39–44.
204 Y. C. Guillaume, L. Lethier and C. Andre, *Chromatographia*, 2018, **81**, 239–245.
205 X. Xiong and M. Qi, *J. Chromatogr. A*, 2018, **1567**, 191–197.
206 J. M. M. Mohamed, F. Ahmad, M. El-Sherbiny, M. A. Al Mohaini, K. Venkatesan, Y. B. A. Alrashdi, M. B. Eldesoqui, A. E. Ibrahim, A. F. Dawood, A. M. Ibrahim and S. El Deeb, *Cancer Nanotechnol.*, 2024, **15**, 16.
207 I. V. Sukhorukova, I. Y. Zhitnyak, A. M. Kovalskii, A. T. Matveev, O. I. Lebedev, X. Li, N. A. Gloushankova, D. Golberg and D. V. Shtansky, *ACS Appl. Mater. Interfaces*, 2015, **7**, 17217–17225.
208 H. Zhang, S. Chen, C. Zhi, T. Yamazaki and N. Hanagata, *Int. J. Nanomed.*, 2013, **8**, 1783–1793.
209 S. Feng, H. Zhang, T. Yan, D. Huang, C. Zhi, H. Nakanishi and X. D. Gao, *Int. J. Nanomed.*, 2016, **11**, 4573–4582.
210 E. S. Permyakova, I. V. Sukhorukova, L. Y. Antipina, A. S. Konopatsky, A. M. Kovalskii, A. T. Matveev, O. I. Lebedev, D. V. Golberg, A. M. Manakhov and D. V. Shtansky, *J. Phys. Chem. C*, 2017, **121**, 28096–28105.
211 E. Mehrjouei, H. Akbarzadeh, A. N. Shamkhali, M. Abbaspour, S. Salemi and P. Abdi, *Mol. Pharm.*, 2017, **14**, 2273–2284.
212 V. Kumar, K. Nikhil, P. Roy, D. Lahiri and I. Lahiri, *RSC Adv.*, 2016, **6**, 48025–48032.
213 P. Ahmad, M. U. Khandaker, N. Muhammad, F. Rehman, Z. Ullah, G. Khan, M. I. Khan, S. Haq, H. Ali, A. Khan, Y. Saeed and M. I. Irshad, *Appl. Radiat. Isot.*, 2020, **166**, 109404.
214 M. Jedrzejczak-Silicka, M. Trukawka, M. Dudziak, K. Piotrowska and E. Mijowska, *Nanomaterials*, 2018, **8**, 605.
215 H. Li, W. Qiao, Y. Shen, H. Xu, Y. Fan, Y. Liu, Y. Lan, Y. Gong, F. Chen and S. Feng, *Pharmaceutics*, 2023, **15**, 1269.
216 W. M. da Silva, T. Hilário Ferreira, C. A. de Morais, A. Soares Leal and E. M. Barros Sousa, *Appl. Radiat. Isot.*, 2018, **131**, 30–35.
217 D. Doğan and A. Ü. Metin, *Mater. Today Commun.*, 2022, **33**, 104807.
218 Z. Çobandede and M. Çulha, *Nanotechnology*, 2024, **35**, 135101.
219 Ö. Muhammed and B. M. BOZER, *Advanced and Contemporary Studies in Natural Science and Mathematics*, **70**.
220 S. C. Yoo, Y. K. Park, C. Park, H. Ryu and S. H. Hong, *Adv. Funct. Mater.*, 2018, **28**, 1805948.
221 A. B. Kakarla and I. Kong, *Nanomaterials*, 2022, **12**, 2069.
222 J. He, X. Zhang, L. Liu, Y. Wang, R. Liu, M. Li and F. Gao, *J. Funct. Biomater.*, 2023, **14**, 181.
223 S. A. Thibeault, C. C. Fay, S. E. Lowther, K. D. Earle, G. Sauti, J. H. Kang, C. Park and A. M. McMullen, *Radiation Shielding Materials Containing Hydrogen, Boron, and Nitrogen: Systematic Computational and Experimental Study*, 2012.
224 A. A. Darwish, M. H. Hassan, M. A. Abou Mandour and A. A. Maarouf, *Comput. Mater. Sci.*, 2019, **156**, 142–147.
225 G. Chen, Y. Wang, Y. Zou, H. Wang, J. Qiu, J. Cao, S. Wang, D. Jia and Y. Zhou, *Chem. Eng. J.*, 2021, **421**, 127802.
226 M. M. Alzahrani, K. A. Alamry and M. A. Hussein, *Results Chem.*, 2025, **15**, 102199.
227 A. D. Kelkar, Q. Tian, D. Yu and L. Zhang, *Mater. Chem. Phys.*, 2016, **176**, 136–142.
228 M. B. Öztürkmen, Y. Öz and N. Dilsiz, *J. Appl. Polym. Sci.*, 2023, **140**, e54639.
229 Y. Shang, G. Yang, F. Su, Y. Feng, Y. Ji, D. Liu, R. Yin, C. Liu and C. Shen, *Compos. Commun.*, 2020, **19**, 147–153.
230 D. Sun, Z. Sun, D. Yang, X. Jiang, J. Tang and X. Wang, *EcoEnergy*, 2023, **1**, 375–404.
231 L. H. Li and Y. Chen, *Langmuir*, 2010, **26**, 5135–5140.
232 B.-H. Xie, X. Huang and G.-J. Zhang, *Compos. Sci. Technol.*, 2013, **85**, 98–103.

233 Z. Kuang, Y. Chen, Y. Lu, L. Liu, S. Hu, S. Wen, Y. Mao and L. Zhang, *Small*, 2015, **11**, 1655–1659.
234 H. Niu, H. Guo, L. Kang, L. Ren, R. Lv, L. Liu, A. Bashir and S. Bai, *Composites, Part B*, 2024, **272**, 111219.
235 D. Mani, R. Qurratulain, S. Anand and S.-R. Kim, *J. Mater. Chem. C*, 2025, **13**, 8890–8933.
236 S. Mateti, I. Sultana, Y. Chen, M. Kota and M. M. Rahman, *Batteries*, 2023, **9**, 344.
237 W. J. Hyun, A. C. M. de Moraes, J.-M. Lim, J. R. Downing, K.-Y. Park, M. T. Z. Tan and M. C. Hersam, *ACS Nano*, 2019, **13**, 9664–9672.
238 E. P. Gilshteyn, D. Amanbayev, A. S. Anisimov, T. Kallio and A. G. Nasibulin, *Sci. Rep.*, 2017, **7**, 17449.
239 J. Joy, E. George, P. Haritha, S. Thomas and S. Anas, *J. Polym. Sci.*, 2020, **58**, 3115–3141.
240 Q.-h. Lin, S. He, Q.-q. Liu, J.-h. Yang, X.-d. Qi and Y. Wang, *Compos. Sci. Technol.*, 2022, **226**, 109528.
241 Z.-G. Wang, W. Liu, Y.-H. Liu, Y. Ren, Y.-P. Li, L. Zhou, J.-Z. Xu, J. Lei and Z.-M. Li, *Composites, Part B*, 2020, **180**, 107569.
242 Z. Wu, J. Dong, X. Li, X. Zhao, C. Ji and Q. Zhang, *Composites, Part B*, 2023, **266**, 111001.
243 L.-H. Zhao, L. Wang, Y.-F. Jin, J.-W. Ren, Z. Wang and L.-C. Jia, *Composites, Part B*, 2022, **229**, 109454.
244 C. Yu, W. Gong, W. Tian, Q. Zhang, Y. Xu, Z. Lin, M. Hu, X. Fan and Y. Yao, *Compos. Sci. Technol.*, 2018, **160**, 199–207.
245 H. Niu, Y. Cao, K. Yang, H. Dong, Q. Cheng and Y. Chen, *Compos. Appl. Sci. Manuf.*, 2026, **200**, 109289.
246 M. Krishnam, S. Bose and C. Das, *Appl. Therm. Eng.*, 2016, **106**, 951–958.
247 A. G. N. Sofiah, R. K. Rajamony, M. Samykano, A. K. Pandey, J. Pasupuleti and N. F. Sulaiman, *Process Saf. Environ. Prot.*, 2024, **189**, 1087–1102.
248 J. Sheng, B. Yan, W.-D. Lu, B. Qiu, X.-Q. Gao, D. Wang and A.-H. Lu, *Chem. Soc. Rev.*, 2021, **50**, 1438–1468.
249 P. Wu, W. Zhu, Y. Chao, J. Zhang, P. Zhang, H. Zhu, C. Li, Z. Chen, H. Li and S. Dai, *Chem. Commun.*, 2016, **52**, 144–147.
250 J. T. Grant, C. A. Carrero, F. Goeltl, J. Venegas, P. Mueller, S. P. Burt, S. E. Specht, W. P. McDermott, A. Chieregato and I. Hermans, *Science*, 2016, **354**, 1570–1573.
251 P. Li, H. Li, X. Pan, K. Tie, T. Cui, M. Ding and X. Bao, *ACS Catal.*, 2017, **7**, 8572–8577.
252 H. Fu, K. Huang, G. Yang, Y. Cao, H. Wang, F. Peng, X. Cai, H. Gao, Y. Liao and H. Yu, *ACS Catal.*, 2021, **11**, 8872–8880.
253 H. Chen, D.-e. Jiang, Z. Yang and S. Dai, *Acc. Chem. Res.*, 2023, **56**, 52–65.
254 T. Agbi, W.-S. Lo, K. Baamran, T. Ryu, C. Cheung, F. Rezaei and I. Hermans, *Top. Catal.*, 2023, **66**, 1152–1160.
255 C. Huang, C. Chen, M. Zhang, L. Lin, X. Ye, S. Lin, M. Antonietti and X. Wang, *Nat. Commun.*, 2015, **6**, 7698.
256 J. Liang, W. Zhang, Z. Liu, Q. Song, Z. Zhu, Z. Guan, H. Wang, P. Zhang, J. Li, M. Zhou, C. Cao, H. Xu, Y. Lu, X. Meng, L. Song, P. K. Wong, Z. Jiang and C.-S. Lee, *ACS Catal.*, 2022, **12**, 12217–12226.
257 A. S. Konopatsky, K. L. Firestein, D. V. Leybo, Z. I. Popov, K. V. Larionov, A. E. Steinman, A. M. Kovalskii, A. T. Matveev, A. M. Manakhov, P. B. Sorokin, D. Golberg and D. V. Shtansky, *Catal. Sci. Technol.*, 2018, **8**, 1652–1662.
258 K.-I. Choi, D. Yadav, J. Jung, E. Park, K.-M. Lee, T. Kim and J. Kim, *ACS Appl. Mater. Interfaces*, 2023, **15**, 10670–10678.
259 H.-G. Im, M.-J. Lee, W.-G. Kim, S.-J. Kim, B. Jeong, B. Ye, H. Lee and H.-D. Kim, *Nanomaterials*, 2022, **12**, 2329.
260 C. J. H. Jacobsen, *J. Catal.*, 2001, **200**, 1–3.
261 K. Uosaki, G. Elumalai, H. Noguchi, T. Masuda, A. Lyalin, A. Nakayama and T. Taketsugu, *J. Am. Chem. Soc.*, 2014, **136**, 6542–6545.
262 J. Dong, L. Gao and Q. Fu, *J. Phys. Chem. Lett.*, 2021, **12**, 9608–9619.